September 7, 2018

Dear Dr. Keenan,

Thank you very much for providing the opportunity to revise the manuscript for consideration of publication in *Biogeosciences*. We would like to express our great appreciation to you and the two anonymous reviewers for their valuable suggestions and comments on the previous version of the manuscript.

We revised the manuscript by addressing all the comments and concerns raised by the reviewers. Specifically, Reviewer #1 asked about the comparison with the SIF* dataset and the time-series comparison with other SIF dataset. In this revised version, we added one figure showing the comparison for 12 major land cover types during the model training and validation. We also revised the figure by adding the comparison with SIF* and time-series comparisons of CSIF, RSIF and SIF*.

We hope that the revised manuscript is satisfactory for you, the reviewers, and *Biogeosciences*. Please feel free to contact me if further information is required. Thank you very much for your consideration. I am looking forward to hearing from you soon.

Yours sincerely,

Yao Zhang

Postdoctoral Research Scientist
Department of Earth and Environmental Engineering
Columbia University
500 W 120th St, 842G
New York, NY 10027

**Anonymous Referee #1**

Received and published: 24 July 2018

Review for "A global spatially Continuous Solar Induced Fluorescence (CSIF) dataset using neural networks" by Yao Zhang et al.

In this work the authors produce three datasets of CSIF by filling spatial and temporal gaps of SIF soundings by OCO2 using MODIS surface reflectances and machine learning. The resulting datasets in 0.05deg and 4-day resolution represent gap-filled instantaneous SIF under cloud-free conditions, cloud-free SIF integrated to a daily value and daily SIF under all-sky conditions. To illustrate the advantages and the usefulness of these high-resolution datasets they compare to another downscaled fluorescence product (RSIF, based on GOME2 and different MODIS reflectance datasets), GOME2 SIF, EC GPP and OCO2-SIF itself based on drought occurrences.

The authors convincingly argue why a new down-scaled SIF product - based on OCO2 as a new factor – is needed. At several points I do see, however, need for clarification (where the authors partly contradict themselves in my opinion), further discussion and analysis.

Response: Thanks for your nice summary. We address your concerns point-by-point below.

The main points are:

1) Does CSIF represent SIF or APARgreen (p. 3 l. 30)? At several occasions in the manuscript (e.g. p.8 l.14, p.11 l.26) the authors state that based on the reflectances SIFyield cannot be reproduced by NN. They base the drought event analysis on this assumption by comparing CSIF to OCO2 SIF (p.10 l.5). At other moments, however, they stress the close relationship of CSIF to SIF (p.8 l. 18, p.11 l. 31) and call it CSIF.

Response: As we discussed in the introduction, $APAR_{chl}$ (or $APAR_{green}$) is the primary driver of the SIF variation at subdaily or seasonal scales (Du et al., 2017). The $SIF_{yield}$, on the other hand, can be relatively stable at monthly or seasonal scales although diurnal variations exist. A recent study using canopy SIF observations at a paddy rice site also showed that SIF is strongly correlated with APAR more so than with GPP at both half-hourly ($R^2$=0.82) and daily ($R^2$=0.85) scale (Yang et al., 2018). However, this only holds when no strong environmental stress is present. When environmental stress exists, the $SIF_{yield}$ should play a more important role and decrease SIF from its normal conditions (Liu et al., 2018).

We call this dataset CSIF since it reproduces most of the SIF variations retrieved by the OCO-2 satellite. The drought may happen for a limited space and time and deviate CSIF from OCO-2 SIF, but the overall relationship between CSIF and OCO-2 SIF is still very close.

Liu, L., Yang, X., Zhou, H., Liu, S., Zhou, L., Li, X., Yang, J., Han, X. and Wu, J.: Evaluating the utility of solar-induced chlorophyll fluorescence for drought monitoring by comparison with NDVI derived from wheat canopy, Science of The Total Environment, 625, 1208–1217, doi:10.1016/j.scitotenv.2017.12.268, 2018.

Yang, K., Ryu, Y., Dechant, B., Berry, J. A., Hwang, Y., Jiang, C., Kang, M., Kim, J., Kimm, H., Kornfeld, A. and Yang, X.: Sun-induced chlorophyll fluorescence is more strongly related to absorbed light than to photosynthesis at half-hourly resolution in a rice paddy, Remote Sensing of Environment, 216, 658–673, doi:10.1016/j.rse.2018.07.008, 2018.

2) Related to point 1, why not compare CSIF to other estimates of APAR? Greenness index * PAR?

Response: Thanks for your suggestion, the comparison between SIF and APAR has been carried out by several other studies both at regional scale (Zhang et al., 2016) and at site level (Yang et al., 2015; Yang et al., 2018). However, accurate acquisition of $APAR_{chl}$ (rather than APAR) that drives the SIF and GPP is problematic. When using $APAR_{canopy}$ observations, the difference between $APAR_{chl}$ and $APAR_{canopy}$ (mostly related to chlorophyll concentration in the canopy) will be mistakenly interpreted as fluorescence yield or light use efficiency (Zhang et al., 2018).

Another problem with greenness index * PAR is that the greenness indices do not align with fPAR at 0. Several studies use different factors to correct for this misalignment, ranging from 0.02 (Ruimy et al., 1994) to 0.28 (Lind and Fensholt, 1999) for NDVI. In essence, this correction factor is affected by the soil (or snow) background and no universal value may be used. CSIF may be able to better capture the soil background information since it is directly trained on OCO-2 SIF, the soil background information can be correctly picked up by the NN and the resulting CSIF can be more closely related to SIF than greenness index * PAR.

Ruimy, A., Saugier, B., & Dedieu, G. (1994). Methodology for the estimation of terrestrial net primary production from remotely sensed data. *Journal of Geophysical Research: Atmospheres*, *99*(D3), 5263-5283.

Lind, M., & Fensholt, R. (1999). The spatio-temporal relationship between rainfall and vegetation development in Burkina Faso. *Geografisk Tidsskrift*, *2*.

Yang, K., Ryu, Y., Dechant, B., Berry, J. A., Hwang, Y., Jiang, C., Kang, M., Kim, J., Kimm, H., Kornfeld, A. and Yang, X.: Sun-induced chlorophyll fluorescence is more strongly related to absorbed light than to photosynthesis at half-hourly resolution in a rice paddy, Remote Sensing of Environment, 216, 658–673, doi:10.1016/j.rse.2018.07.008, 2018.

Yang, X., Tang, J., Mustard, J. F., Lee, J., Rossini, M., Joiner, J., Munger, J. W., Kornfeld, A. and Richardson, A. D.: Solar-induced chlorophyll fluorescence that correlates with canopy photosynthesis on diurnal and seasonal scales in a temperate deciduous forest, Geophysical Research Letters, 42(8), 2977–2987, doi:10.1002/2015GL063201, 2015.

Zhang, Y., Xiao, X., Jin, C., Dong, J., Zhou, S., Wagle, P., Joiner, J., Guanter, L., Zhang, Y., Zhang, G., Qin, Y., Wang, J. and Moore, B.: Consistency between sun-induced chlorophyll fluorescence and gross primary production of vegetation in North America, Remote Sensing of Environment, 183, 154–169, doi:10.1016/j.rse.2016.05.015, 2016.

Zhang, Y., Xiao, X., Wolf, S., Wu, J., Wu, X., Gioli, B., Cescatti, A., Van Der Tol, C., Zhou, S., Gough, C., Gentine, P., Zhang, Y., Steinbrecher, R. and Ardö, J.: Spatio-temporal convergence of maximum daily light-use efficiency based on radiation absorption by canopy chlorophyll, Geophysical Research Letters, (45), 3508–3519, doi:10.1029/2017GL076354, 2018.

3) Temporal resolution: The final data sets are claimed to have 4day temporal resolution. What is left unmentioned in the manuscript is that the MCD43C4 reflectance data have daily sampling, but each value for a given day still represents a 16-day period (weighted to the central date). So the 4-daily temporal resolution might in reality represent periods of 19days length and potentially affect the downscaling and all comparisons. Please consider this in your evaluations and discussion.

Response: Thanks for your suggestion, we also realized that the MCD43C4 dataset uses 16 days of data as input and the day of interest is emphasized. This may cause potential temporal inconsistency in the dates it represents. However, we think this would have limited effect due to the following reasons: (1) the vegetation growth is continuous in time, the optical properties that will be obtained by satellite would not change abruptly. (2) although MCD43C4 uses 16-day worth of inputs, it also emphasizes the day of interest. Nevertheless, we agree this should be made clear in the revised manuscript and we added the discussions of this issue in the Method section 2.2.

4) Although data processing is described in detail, at points clarification is necessary (e.g. regarding temporal aggregation for training, quality filters of reflectance and EC GPP data, see below).

Response: We tried to resolve your concerns and clarify the data filtering issues.

5) Spatial splitting for training-validation in addition to the temporal one, as extrapolation is not only done in time but also in space. I put it here as a recommendation.

Response: Since the largest variation in vegetation activity are the spatial and seasonal variability, splitting samples by years will maximize the spatial and seasonal coverage in the training and validation samples. In addition, since we need to randomize all the samples prior training the NN, using samples from entire years tend to get more randomly distributed samples in the space-season domain. If we separate the samples by latitude, there may be ecosystems/areas that only occur in the validation but not the training dataset, and the model may be biased.

6) I miss plots of time series throughout the manuscript both regarding training/validation as well as comparisons to other datasets. Such plots could contribute to supporting CSIF as a very useful dataset.

Response: We agree that such time series plots would be helpful to get a sense of seasonal variations. We therefore added a figure for the training and validation dataset (see Figure R2 below). We also revised the figure for the RSIF and SIF* comparison and added the time-series comparison in addition to the regression analysis (Figure R1).

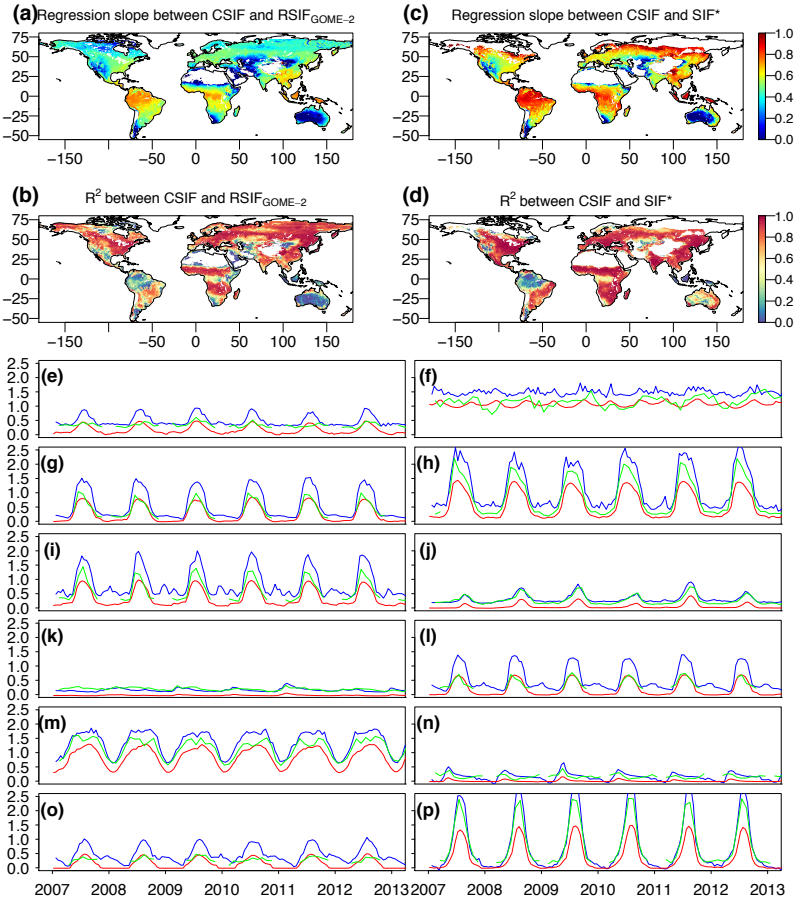

Figure R1. Comparison between CSIF, $RSIF_{GOME-2}$ and SIF* dataset. Regression slopes and coefficient of determination ($R^2$) between the contiguous clear-sky condition instantaneous SIF from OCO-2 ($CSIF_{inst-clear}$) and the reconstructed SIF from GOME-2 ($RSIF_{GOME-2}$ a, b) or SIF* (c, d) dataset. The regressions are forced to pass the origin. The $CSIF_{clear-inst}$ is aggregated to semi-monthly or monthly and $0.5° \times 0.5°$ spatial resolution to be consistent with $RSIF_{GOME-2}$ and SIF*. Comparison uses the data between 2007 to 2016 (RSIF) or 2007 to 2013 (SIF*). White regions are barren regions. (e-p) Time series comparison among CSIF (red), $RSIF_{GOME-2}$ (blue) and SIF* (green) for pixels in 12 major land cover types shown in Figure R2.

7) Related to point 2: An interesting comparison next to the one to RSIF and GOME2

SIF v27 would also be the one to SIF* by Duveiller and Cescatti 2016 that you cite several times.

Response: Thanks for your suggestions, we added this comparison in the revised manuscript (Figure 9).

ad 4)

a) Which period exactly do the OCO2 SIF data cover? It was launched only in Septem- ber 2014, so only a few months of this year are available. Do you use the full year of 2017?

Response: We used the data between September 2014 to December 2017. This has been clarified in the revised manuscript. It is normal to have less samples for validation than for training.

b) Aggregation of OCO2 SIF (p.4 l. 29-p.5 l.18): How do you aggregate in time? Daily, 4-daily?

Response: The aggregation is conducted for each OCO-2 SIF files (daily), since the revisit cycle of OCO-2 SIF is 16 days, and only nadir view SIF observations were used, using daily or 4-day aggregation should not change the value of the samples.

c) Figure 1 nicely shows the spatial distribution of the training and validation data. What does the temporal distribution and representativeness look like? A lat-time plot might be useful here. Why are there no data for validation in Alaska and eastern Siberia?

Response: In Figure 1 (a,b), the color of the dots represents the observations' day of year. Although these dots overlapped in the lower latitude, most of the lower latitude have training and validation samples throughout the year. The boreal regions only have samples during the summer where sun zenith angle is relatively low and no snow or ice cover.

Since the OCO-2 satellite was launched in July 2014 and starting to obtaining data after September that year, limited observations is acquired in boreal regions that year. In 2017, the satellite also experienced malfunctioning in August and early September, making limited observations in the boreal growing season.

d) You might consider removing barren areas in Sahara and central Asia from the analysis to potentially obtain clearer signals as many data points are obtained from these areas (Fig.1) and might affect the relationships in Fig.2-4.

Response: We agree that using the non-barren samples to train the dataset may yield slightly better performance. However, in this study, we aim to generate a global spatially continuous dataset. The SIF dynamic in these sparsely vegetated may be potentially of interest to future studies. Therefore, using the training samples from these regions are necessary.

e) p.5 ll. 12-17: If you first aggregate several soundings to 0.05deg and only afterwards integrate to a daily value, which SZA of the measurement do you use?

Response: If we call a 0.05-degree aggregated pixel a training sample, all the retrievals to generate this sample are from the consecutive observations within a very short period of time, usually within several seconds. The SZA during this period have little change and the average SZA from these retrievals is used as the SZA of this aggregated sample.

f) p.5 l. 21 and at several other occasions in the manuscript: which is the period covered? 2000-2017 or 2001-2016 (abstract) for CSIF?

Response: The clear-sky instantaneous/daily CSIF only requires surface reflectances and calculated SZA as input, therefore, these two datasets span from 2000 to 2017. Limited by the availability of BESS PAR (2000-2016), the all-sky daily CSIF only span from 2000-2016. We have corrected the data coverage throughout the manuscript.

g) Processing of reflectance data: Do you apply any quality filters? You mention the 'best atmospheric conditions' (p. 6 l. 7), what did you do? I am wondering how can you obtain 'more realistic prediction of SIF during winter' if the reflectances do not represent vegetation but snow? MCD43C4 is sampled daily but values represent 16 days worth of data.

Response: The MCD43C4 dataset has filtered out bad estimates (cloud affected) during the pre-processing for the model inversion (Schaaf et al., 2002), therefore no additional quality check is applied in this study. However, the MCD43C4 also suffers from spatial gaps caused by failing to implement the inversion model and predict the NBAR. To fill the gaps in the MCD43C4 dataset, we used the algorithm (Zhang et al., 2017) for each band to reconstruct the 4-day observations.

Since the RossThick/LiSparse-Reciprocal BRDF model used to generate MCD43C4 dataset may fail under contaminated atmospheric conditions, the observations obtained at bad atmospheric conditions is likely to be filter out during the model inversion and aggregation processes. We realized that this statement is not accurate and we have revised this to:

*"Since this processing does not involve any extra information and only uses the reflectance observations from the successful model inversion, it should be comparable to the reflectance used for NN training."*

We deliberately included the snow affected pixels in the training and prediction, so that if the pixel is covered by snow (usually have quite different surface reflectances than vegetated surface), its SIF values can be correctly predicted. If the vegetation is covered by snow, it is likely to have minimum APAR and little SIF, both spectral observation (reflectance) from MODIS and SIF from OCO-2 would contain little vegetation signal. This enables us to get consistent SIF values with the satellite retrievals.

We added some discussion about the temporal representation of MCD43C4 in Section 2.2

Zhang, Y., Xiao, X., Wu, X., Zhou, S., Zhang, G., Qin, Y. and Dong, J.: A global moderate resolution dataset of gross primary production of vegetation for 2000–2016, Scientific Data, 4, 170165, doi:10.1038/sdata.2017.165, 2017.

Schaaf, C. B., Gao, F., Strahler, A. H., Lucht, W., Li, X., Tsang, T., Strugnell, N. C., Zhang, X., Jin, Y., Muller, J.-P., Lewis, P., Barnsley, M., Hobson, P., Disney, M., Roberts, G., Dunderdale, M., Doll, C., d'Entremont, R. P., Hu, B., Liang, S., Privette, J. L. and Roy, D.: First operational BRDF, albedo nadir reflectance products from MODIS, Remote Sensing of Environment, 83(1–2), 135–148, doi:10.1016/S0034-4257(02)00091-3, 2002.

h) You might consider adding a few sentences on BESS PAR in addition to citing Ryu et al. 2018. The quality of BESS PAR is not discussed in the discussion part.

Response: We have now added several sentences in Section 4.4 to discuss the quality of BESS PAR dataset and its effect on CSIF.

i) In the comparisons to GOME2 SIF v27 and RSIF, is there any accounting for over- pass time and wavelength necessary between GOME2 and OCO2? A comparison to SIF* by Duveiller and Cescatti would complete the suite of products.

Response: We did not consider the differences of SIF emission at 757nm and 740nm. Since the regression is conducted at the temporal domain for each pixel, the temporal variation of ratio between SIF at 757nm to SIF at 740nm is thought to be limited and does not affect the coefficient of

determination. Since all the comparisons uses the daily averaged SIF, there is no need to consider the overpass time differences.

We did not add the SIF* dataset into comparison in the first version of the manuscript since it is not open to the public. In this revised version, we added the comparison between CSIF and SIF* together with the RSIF dataset. We also added a paragraph to describe this results in Section 3.3

j) EC GPP: Please add a bit more information: Did you use FLUXNET 2015 or the LaThuile data set? Is there any reason for choosing nighttime partitioning? l. 28-30: I would think you retain those data?

Response: We used the FLUXNET2015 dataset. This is made clearer in the revised manuscript. The nighttime partitioning method is now better described and can be regarded as more independent estimate of GPP. The daytime method assumes a hyperbolic dependence of PAR which also affect SIF. However, the difference between these two is minor (see the detailed comparison in Zhang et al., 2018).

Yes, we do mean those data are retained. This has been corrected in the revised manuscript.

Zhang, Y., Xiao, X., Zhang, Y., Wolf, S., Zhou, S., Joiner, J., Guanter, L., Verma, M., Sun, Y., Yang, X., Paul-Limoges, E., Gough, C. M., Wohlfahrt, G., Gioli, B., van der Tol, C., Yann, N., Lund, M. and de Grandcourt, A.: On the relationship between sub-daily instantaneous and daily total gross primary production: Implications for interpreting satellite-based SIF retrievals, Remote Sensing of Environment, 205, 276–289, doi:10.1016/j.rse.2017.12.009, 2018.

Training and validation (p. 8 ll. 1-26):

-Time series of the CSIF during validation would be nice to see, with validation points overlaid, for example to illustrate the point of SIFyield in SV and GRA.

Response: We agree that the time series validation of the CSIF data would be a great complimentary to the scatter plot and the boxplot, here we select 12 2°×2° gridboxes, and plot their time-series for the SIF retrieval from OCO-2, and CSIF predicted values for the corresponding pixels and date. The CSIF generally showed minimum differences from the original OCO-2 SIF, except slight underestimation during the peak growing season for cropland and deciduous broadleaf forest for some years. Since the $SIF_{yield}$ may only have significant effect during strong environmental stress period, which will be further shown and discussed in Section 3.4 and 4.2, we did not deliberately select samples that are affected by the drought.

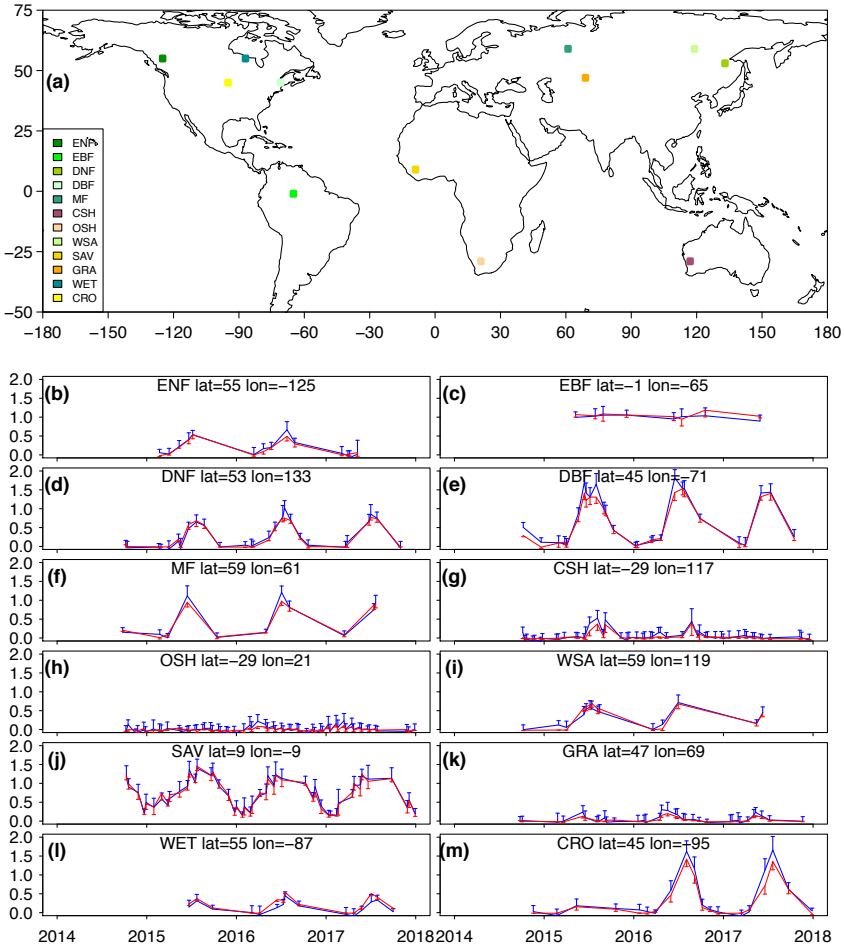


Figure R2. Comparison of predicted SIF by NN and OCO-2 observed SIF for 12 samples (2° ×2°) of major vegetated land cover types during 2014 to 2017. All samples in the training and validation are used. The blue color represents the observed SIF by OCO-2 and the red color represent the SIF prediction by NN. The error bars represent the standard deviation of all 0.05° ×0.05° samples used to generate the 2° ×2° gridboxes. MODIS MOD12C1 V6 land cover dataset is used to select these sample gridboxes.

-Also crops are strongly biased.

Response: Thanks for pointing out, we also described and discussed this in the revised manuscript.

-l.17-19: At other points it is argued that CSIF cannot accurately reproduce SIFyield effects based only on reflectances. Please clarify and discuss.

Response: Through a sensitivity test using the SCOPE model, the fluorescence yield variations under unstressed conditions are small, especially compare to the variation of APAR. This is also supported by a recent study carried out at a paddy rice cropland, suggesting that SIF contains most information of APAR than GPP (Yang et al., 2018). The short-term variations of fluorescence yield may be significant and become important when strong stress presents (Frankenberg et al., 2017), which is not prevalent for the training samples. The long-term (seasonal) or cross-biome changes in fluorescence yield may be related to leaf nitrogen content or carboxylation rate that may be in embedded in the surface reflectance and implicitly picked up by the Neural Network.

We highlighted the differences between the mean fluorescence yield and stress induced fluorescence yield changes in the revised manuscript.

Frankenberg, C. and Berry, J. A.: Solar Induced Chlorophyll Fluorescence: Origins, Relation to Photosynthesis and Retrieval, in Comprehensive Remote Sensing, pp. 143–162, Elsevier., 2017.

Drought monitoring application:

-Please consider the different temporal information in instantaneous OCO2 SIF versus CSIF based on 19 days worth of data and take it into account and/or discuss it.

Response: Thanks for your suggestion. Since during the drought period, the atmospheric conditions are less likely to be contaminated and the MCD43C4 dataset tends to give the best estimate using the full model inversion with the day of interest highlighted. This reduced the possibility of using observations far from the day of interest.

We agree this could be an important issue for the drought monitoring using CSIF. We therefore added some discussion in Section 4.2 about this issue.

*"MCD43C4 dataset uses 16 days of inputs for the model inversion, although this may lead to temporal inconsistency for the comparison between CSIF and OCO-2 SIF, it may have limited effect due to the higher data quality during drought with less cloud coverage."*

-It would also be interesting to see here a comparison (although I see that the different temporal resolutions would mean more work) also to an estimate of APAR, RSIF, OCO2 SIF/ APAR and SIF* by Duveiller & Cescatti 2016.

Response: Thanks for your suggestion. For the drought monitoring, as we discussed later in the Section 4.2, we would like to highlight the different basis for two drought monitoring methods, the VI based ones use interannual anomalies and detect drought only at later stage. The CSIF based method focuses more on the physiological stress on fluorescence yield. Adding additional APAR dataset would

introduce uncertainties related to both PAR and fPAR ($fPAR_{chl}$ and $fPAR_{canopy}$, see our response to comments related Sims et al., 2005). In addition, the SIF* dataset does not have coverage for the period of interest.

A few questions when reading the Discussion:

4.1. What is the advantage of CSIF compared to using vegetation index * PAR?

Response: please refer to our responses to the first two comments about the difference between CSIF and vegetation index*PAR

Is there a trend in RSIF?

Response: Since RSIF starts from January 15th 2007, we only have 9 full years to calculate the trend for the RSIF, which is much shorter than CSIF dataset. The spatial patterns are somewhat similar, for example a positive trend in Europe, southeast China, North India, and a negative trend in East Brazil. Since RSIF is not the focus of this study and the comparison is during different period of time, we did not include this figure in the paper.

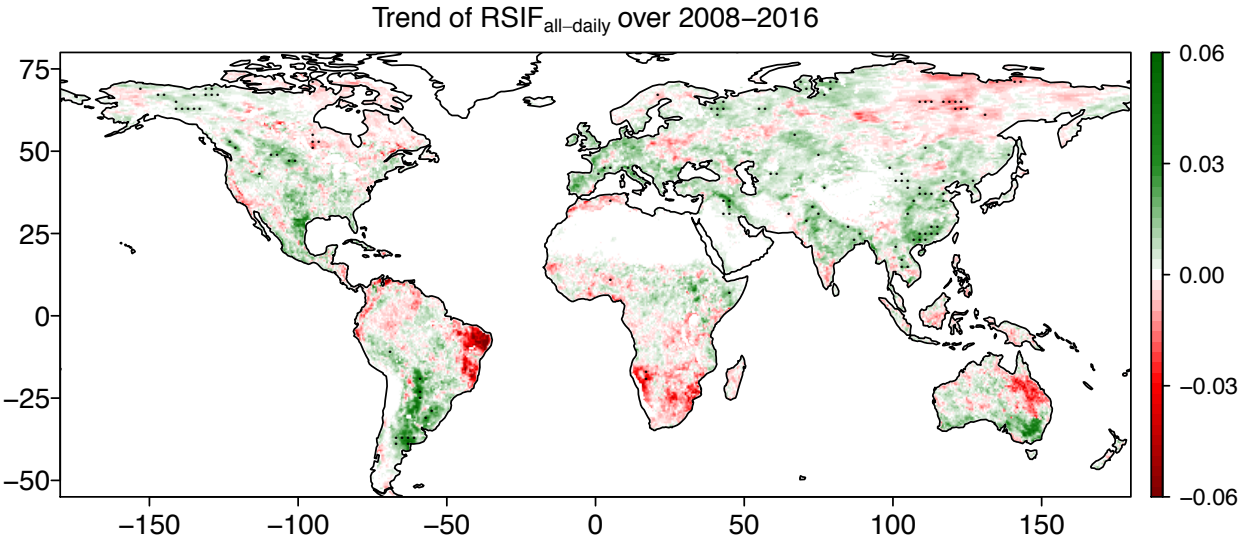


Figure R2. The trend of RSIF during 2008 to 2016. Black dots represent trend is significant at P<0.05 through the Mann-Kendall test. The trend is estimated by the Sen's slope estimator.

4.2. Although I fully agree, vegetation indices might not be completely blind. Sims et al. 2006 (RSE, 10.1016/j.rse.2005.01.020) argue that for some ecosystems vegetation indices can contain information on photosynthetic yields.

Response: We agree that several studies including Sims et al., 2006; Wu et al., 2010 suggested that the vegetation indices (VI) have positive correlation with the light use efficiency and a VI model is further developed. However, we argue that these positive correlations may be caused by different definitions of light use efficiency (Gitelson and Gamon, 2015; Zhang et al., 2018). The fraction of light absorbed by the canopy chlorophyll ($fPAR_{chl}$) is what drives the photosynthesis, but it is only a proportion of the total light absorbed by canopy ($fPAR_{canopy}$). There may be positive correlations between the ratio of these two FPAR definitions ($fPAR_{chl}$/ $fPAR_{canopy}$) and the VI, but the correlation between these two does not support the usage of VI for plant physiological stress, which is also suggested by Sims et al., 2005, as the correlation break down during drought. In other words, the VIs may correlate with the seasonal changes of chlorophyll concentration, but the yield information is only related to the energy partitioning after absorption by photosystems by its definition, and should be independent from the canopy characteristics.

Wu, C., Niu, Z. and Gao, S.: Gross primary production estimation from MODIS data with vegetation index and photosynthetically active radiation in maize, Journal of Geophysical Research Atmospheres, 115(12), 1–11, doi:10.1029/2009JD013023, 2010.

Gitelson, A. A. and Gamon, J. A.: The need for a common basis for defining light-use efficiency: Implications for productivity estimation, Remote Sensing of Environment, 156, 196–201, doi:10.1016/j.rse.2014.09.017, 2015.

Zhang, Y., Xiao, X., Wolf, S., Wu, J., Wu, X., Gioli, B., Cescatti, A., Van Der Tol, C., Zhou, S., Gough, C., Gentine, P., Zhang, Y., Steinbrecher, R. and Ardö, J.: Spatio-temporal convergence of maximum daily light-use efficiency based on radiation absorption by canopy chlorophyll, Geophysical Research Letters, (45), 3508–3519, doi:10.1029/2017GL076354, 2018.

4.3. In far-red SIF reabsorption should play a very minor role compared to scattering.

Response: Thanks for your suggestion, we agree that the reabsorptions are relatively small at far-red SIF and recent studies suggest scattering is important for SIF at far-red wavelength (Yang et al., 2018). We revised these sentences to make them accurate.

I am afraid I do not understand the last paragraph (specifically p.14 ll. 12-15). Please rephrase.

Response: We rewrote this paragraph in the revised version of the manuscript. It should be clearer now.

Minor:

P.6 l. 3: In the end four bands are used, not seven.

Response: revised as suggested.

Fig.6a) There are also low values in 2007 and 2010 and high values in 2011 compared to 2010 and 2012 during La Nina in Australia at 40S.

Response: Thanks for pointing out, since the austral summer is between the two years, we revised this sentence to accurately describe the dry and wet years.

*"Low SIF values can be found in dry years (2006-2007, 2009-2010) while high values were observed in wet or normal years (2010-2011, 2012-2015)."*

Fig.9 Maybe exclude SAA from the plot as GOME2 v27 will be affected by it. p.10 l. 27: somehow there are too many numbers.

Response: Thanks for your suggestions, we agree that GOME-2 SIF in parts of South America is affected by the SAA. SIF retrievals from these areas has high uncertainty, and the correlation between CSIF and GOME-2 SIF is much lower than other regions that have similar seasonal variability. We decided to keep the comparison in this region since it is interesting when comparing with the RSIF for the same region. We added additional sentences describing this phenomenon and its causes.

We also corrected the slope range issues for the $CSIF_{site}$.

Fig. 10: I recommend a clearer white for the zero values, the gray is difficult to distinguish from the red and blue for small values.

Response: We revised this figure as suggested. However, to make these white points distinguishable, we changed the background to dark grey.

Discussion of uncertainties in BESS PAR is missing.

Response: Thanks for pointing out, we added the discussion about BESS PAR performance in Section 4.4

Conclusion:
MCD43C4 is based not only on Aqua.

Response: We have removed Aqua in this sentence.

p. 15 l. 19: 0.5 deg or 0.05deg?

Response: The 0.5-degree dataset is provided through Figshare. The raw 0.05-degree dataset exceeded the storage limit and can be obtained upon request. We added this information in the revised text.

p. 15 l. 27: beam radiation
subscripts sb and sd are sometimes incorrect/the same

Response: two misuses of sb are corrected.

For me, calling the SIF multiplied by a daily correction factor 'daily average SIF' is confusing. It is rather an integration over the day, 'daily integrated SIF'.

Response: We followed the OCO-2 SIF user guide (https://docserver.gesdisc.eosdis.nasa.gov/public/project/OCO/OCO2_SIF_B7000_Product_Description_090215.pdf) and name it daily average SIF. It makes sense calling it daily average since the output represents average SIF over 24 hours, although SIF values are 0 during the night.

Are there any applications or areas for which you would not recommend the use of CSIF?

Response: As we have discussed, the CSIF dataset uses only the spectral information and is not suitable to extract plant physiological information by using it alone.

**Anonymous Referee #2**

Received and published: 9 August 2018

In this study authors demonstrate the possibility of generating contiguous, high resolution estimates of SIF utilizing machine leaning, using as inputs sparse available OCO- 2 SIF retrievals and ancillary satellite data (MODIS). Authors provided extensive error statistics and demonstrated applicability of the new approach in identifying/studying effects of drought. The study is well written and suffers only from minor issues.

Response: We thank the reviewer for the clear summary and positive comments.

Page 1, Line 10-11: "However, several issues, including low spatial and temporal reso- lution of the gridded datasets and high uncertainty of the individual retrievals, limit the applications of SIF.

Reviewer: Binned/averaged datasets are not the only option, there is entire family of products based on geostatistics/kriging (i.e. Tadic et al, 2017), so it could be nice to compare weaknesses/advantages to those products as well.

Response: Thanks for your suggestion. Indeed, geo-statistics is another option to generate high resolution contiguous SIF dataset. However, considering that we already have quite a few contents in this study, and the comparison between different methods in generating high resolution SIF dataset can foster an independent study, we decided not adding the comparison in this paper. Yet, we mention that some other family of products could be used.

Page 1, Lines 14-15: "....we generated two global spatially continuous SIF (CSIF) datasets at moderate spatio-temporal resolutions (0.05 degree 4-day). . ."

Reviewer: How did you choose the ST resolution? Why 4-day? Is it based on the expected decoorelation lenght (variability) in time? Why not 1*day?

Response: The spatial resolution of 0.05 is fine enough for comparison with site level observations (compared with swath based OCO-2 SIF), it also provides global coverage without dividing the Earth surface into tiles (like the 500m MODIS dataset), which simplifies the global application. In addition, many input datasets are available at the 0.05 degree (BESS PAR for example).

We chose this temporal resolution to reach a balance among applications requirements, information redundancy, and dataset sizes. For most GPP dataset, they are either 8-day or monthly temporal resolution. For widely used SIF datasets, GOME-2 for example, they are mostly at the monthly or semi-monthly resolution. Since SIF is often used as a reliable proxy of APAR or GPP, and both of which do

not change abruptly, to get the seasonal or spatial variation, the 4-day temporal resolution is adequate. Although higher temporal resolution may be obtained using the MODIS MCD43C4 dataset, larger spatial gaps caused by the low data quality (cloud, high aerosols) need to be filled. The information redundancy increases if excessive interpolation is applied. In addition, the MODIS MCD43C4 uses 16 days of input with the day of interest emphasized. This reduced the reliability of using MCD43C4 to represent the actual reflectance for the target date. Using 4-day temporal resolution will also decrease the dataset size compared to using a higher temporal resolution, and it is easy to aggregate and compare with other GPP dataset at 8-day or monthly temporal resolution.

Page 3, Lines 24-26: "In addition, OCO-2 can only generate a gridded monthly dataset at relatively coarse spatial resolution, typically at1°×1°, which limits its application in small regions. "

Reviewer: This is not quite correct. It is correct only if we limit our approach to bin- ning/averaging, and ignore spatial autocorrelations. However, if we take autocorre- lations into account, we get have estimates at much higher spatio-temporal resolu- tions (see Tadic et al, 2015, doi:10.5194/gmd-8-3311-2015âA˘ land Tadic et al, 2017, doi:10.5194/gmd-10-709-2017)

Response: We agree that using geo-statistical methods, we can get higher spatial-temporal dataset from low resolution dataset. These methods are effective when the spatial autocorrelations are high (e.g., for atmospheric gases or atmospheric temperature). However, the surface vegetation heterogeneity is high especially in the presence of land use and land cover changes, making this method less applicable. Considering the large gaps between OCO-2 swaths (~100 km), using statistical method without additional information to generate high resolution SIF dataset from OCO-2 SIF would suffer from high uncertainty. Nevertheless, we revised this sentence to make it accurate, we also discussed the challenges of using statistical method to downscale the OCO-2 SIF dataset and cite the references suggested by the reviewer.

*"Although several statistical methods are proposed to downscale satellite observations to finer spatial-temporal resolutions (Tadić et al., 2015, 2017), considering the land surface heterogeneity and wide gaps between OCO-2 swaths (~ 100 km), it could be challenging to apply these methods to OCO-2 SIF."*

We also discussed the possibility of using geostatistical method to generate spatially contiguous drought monitoring dataset in Section 4.2:

*"The spatial coverage issues can be further improved using the geostatistical based method (Tadić et al., 2017), but this may need further investigation."*

Page 4, Line 17:" In this study, we aim to generate a global continuous SIF (CSIF) product. . ."

Reviewer: Here and throughout the text, perhaps better choice of word would be con- tiguous. Continuous implies that there is an infinite number of estimation locations, while in practice your estimation interval is determined by the granularity of input data, in this case MODIS retrievals.

Response: Thanks for your suggestion, we use the word continuous to distinguish from the swath based, 16-day revisit cycle OCO-2 SIF data. We agree that "contiguous" is more precise and we have revised the title and other occurrences throughout the manuscript.

Page 4, Line 32:" The reasons for using this resolution include: (1) it is directly compa- rable to the OCO-2 SIF footprint s

Reviewer: This statememnt is questinable, 5x5 gives 25km2 footprint, and OCO-2 footprint is less than 3km2 in size. 8 times difference might or might not be viewed as significant.

Response: We agree that, in terms of the area, 8 times difference can be regarded as significant. However, compared to other OCO-2 SIF aggregations (to 1 degree or 2 degree), they are still in the same order of magnitude. And OCO-2 retrievals can be much more representative for the gridcells SIF values of 0.05*0.05 than 1*1 or 2*2 degree. If we reduce the pixel sizes, we may get very few observations within each pixel and would not effectively reduce the uncertainty. We clarified this statement and have rewritten it as:

*"it is directly comparable (in the same order of magnitude) to the OCO-2 SIF footprint size (around 1.3km×2.25km) and the samples within each gridcell can be more evenly distributed and, thus, more representative of the gridcell SIF values than using much coarser* $1° \times 1°$ *or* $2° \times 2°$ *grids"*

Page 5, Lines 3-4:" assuming independent estimates and homogeneous SIF value within each gridcell. . ."

Reviewer: Here an additional assumption is required - the SIF has to be not only homogeneous (spatial dimension) but also constant in time.

Response: Since the aggregation is conducted for each day, that is, all the OCO-2 SIF retrievals used to calculate the average of the 0.05 by 0.05 gridcell are obtained with in a very short period of time (usually within several seconds). As long as we assume that SIF is homogeneous, this aggregation process can be regarded as multiple measurements of the same SIF source.

Page 6, Line 1:" For prediction, we first aggregated the daily reflectance to 4 days. " Reviewer:Why 4?

Response: We chose 4-day temporal resolution for the CSIF dataset as a balance between application requirements, information redundancy, and dataset sizes. We refer the reviewer to the previous responses for details.

We added a brief explanation why 4-day temporal resolution is used in this study.

Page 6, Lines 10-11:" A feedforward neural network (NN) is a number of computational nodes (called neurons) structured in a multi-layer architecture."

Reviewer:In principle, NN can be a single layer structure.

Response: Thanks for pointing this out, we have revised this sentence to

*"A feedforward neural network (NN) is a number of computational nodes (called neurons) structured in a single or multi-layer architecture"*

Page 6, Line 16:" The rectified linear unit (ReLU) was used as the activation " Reviewer:Is there any particular reason for this choice?

Response: The ReLU is frequently used as activation function for scientific research, although in computer sciences, sigmoid functions are also used for classification problems. Overall, ReLU has shown better performance than sigmoid functions in our application but also in most other ones. We now clarify this point further.

Page 7, Lines 14-15:" RSIFGOME-2 (Gentine and Alemohammad, 2018a) uses a similar machine learning technique approach to CSIF but the 15 training is based on the bi-weekly gridded SIF product from GOME-2, and 8-day MYD09A1 reflectance dataset. "

Reviewer: This choice is surprising, as GOME-2 Level 3 products cn be obtained at much higher temporal resolutions, even daily, like it was demonstrated at Tadic et al., 2017. In this case, an unnecessary degradation of information content is induced, as temporal SIF variations during biweekly periods are converted into noise. Given large footprint on GOME-2 retrievals, ML processing here played the role of the downscaling as well, which itself is a challenging process.

Response: We believe that the RSIF dataset has its merits of reducing the uncertainties in raw GOME-2 SIF dataset and downscale GOME-2 SIF to higher spatial resolution. We agree that during this process, the within month variation are partly regarded as the noises, but this has limited effects since the GOME-2 SIF has relative high uncertainties for each individual observation. Since this was performed

in another study we think it is beyond the scope of the current manuscript, but we clarify the point suggested by the reviewer.

Page 8, Lines 1-6

Reviewer: More details are needed here, for the sake of reproducibility. Did you use regularization? What kind of regularization? L2, dropout, their parametrizatuon? How many epochs? Did you use test/validation sets approach or only test?

Response: We did not use dropouts nor other regularization method since the network was not very deep and there was no sign of overfitting. We used 50 epochs with a batch size of 1024 for the training. Only test approach is used. These are now clarified in the text.

Page 10. Line 8:" Figure 10 shows the difference between instantaneous clear-day OCO-2 SIF and CSIFclear-inst. "

Reviewer: Using contiguous Level 3 products based on OCO-2 data and spatio- temporal kriging would yield a figure equivalent to Fig 10, but contiguous.

Response: We thank the reviewer for the suggestion, as we have discussed previously, the application of spatio-temporal kriging to OCO-2 SIF may be challenging and beyond the scope of this study. Here we are only exploring the possibility of using the difference between SIF and CSIF to detect drought. Nevertheless, it could be a very interesting study for the future to map drought impact contiguously using the spatial-temporal kriging. We now acknowledge this in the text.

# A global spatially ~~Continuous~~ Contiguous Solar Induced Fluorescence (CSIF) dataset using neural networks

Yao Zhang[1], Joanna Joiner[2], Seyed Hamed Alemohammad[3], Sha Zhou[1], Pierre Gentine[1,4]

[1]Department of Earth and Environmental Engineering, Columbia University, New York, NY 10027, USA
[2]NASA Goddard Space Flight Center, Greenbelt, MD 20771, USA
[3]Radiant.Earth, Washington, D.C. 20005, USA
[4]Earth Institute, Columbia University, New York, NY 10027, USA

*Correspondence to*: Yao Zhang (zy2309@columbia.edu)

**Abstract.** Satellite-retrieved Solar Induced Chlorophyll Fluorescence (SIF) has shown great potential to monitor the photosynthetic activity of terrestrial ecosystems. However, several issues, including low spatial and temporal resolution of the gridded datasets and high uncertainty of the individual retrievals, limit the applications of SIF. In addition, inconsistency in measurements footprints also hinder the direct comparison between gross primary production (GPP) from eddy covariance (EC) flux towers and satellite-retrieved SIF. In this study, by training a neural network (NN) with surface reflectance from the MODerate-resolution Imaging Spectroradiometer (MODIS) and SIF from Orbiting Carbon Observatory-2 (OCO-2), we generated two global spatially ~~continuous~~ contiguous SIF (CSIF) datasets at moderate spatio-temporal resolutions (0.05 degree 4-day) during ~~2001-2016~~the MODIS era, one for clear-sky conditions (2000-2017) and the other one in all-sky conditions (2000-2016). The clear-sky instantaneous CSIF ($CSIF_{clear\text{-}inst}$) shows high accuracy against the clear-sky OCO-2 SIF and little bias across biome types. The all-sky daily average CSIF ($CSIF_{all\text{-}daily}$) dataset exhibits strong spatial, seasonal and interannual dynamics that are consistent with daily SIF from OCO-2 and the Global Ozone Monitoring Experiment-2 (GOME-2). An increasing trend (0.39%) of annual average $CSIF_{all\text{-}daily}$ is also found, confirming the greening of Earth in most regions. Since the difference between satellite observed SIF and CSIF is mostly caused by the environmental down-regulation on $SIF_{yield}$, the ratio between OCO-2 SIF and $CSIF_{clear\text{-}inst}$ can be an effective indicator of drought stress that is more sensitive than normalized difference vegetation index and enhanced vegetation index. By comparing $CSIF_{all\text{-}daily}$ with gross primary production (GPP) estimates from 40 EC flux towers across the globe, we find a large cross-site variation (c.v. = 0.36) of GPP-SIF relationship with the highest regression slopes for evergreen needleleaf forest. However, the cross-biome variation is relatively limited (c.v. = 0.15). These two ~~continuous~~ contiguous SIF datasets and the derived GPP-SIF relationship enable a better understanding of the spatial and temporal variations of the GPP across biomes and climate.

## 1 Introduction

Obtaining a spatio-temporal continuous photosynthetic carbon fixation or gross primary production (GPP) dataset is crucial to food security, ecosystem service and health evaluation, and global carbon cycle studies (Beer et al., 2010). However, this

is not possible without remote sensing data, since *in situ* carbon flux measurements, such as FLUXNET (Baldocchi et al., 2001), are usually costly and have limited spatial and temporal coverages (Schimel et al., 2015). Many remote sensing based productivity efficiency models (PEMs) have been built, but the model structure and parameterizations differ from each other and the performance of most models is not satisfactory in terms of simulated inter-annual variability and trends (Anav et al., 2015; Chen et al., 2017).

Müller (1874) found that the chlorophyll fluorescence (ChlF) from a dilute chlorophyll solution was much stronger than the ChlF from a green leaf, suggesting that an alternative energy pathway exists for leaves *in vivo*. In the 1980s, scientists found that plant photosynthesis and heat dissipation are two alternatives to quench the excited chlorophylls, and there is a close linkage between ChlF and carbon assimilation rate (Genty et al., 1989; Krause and Weis, 1991). Leaf-level photosynthesis ($A_{leaf}$) and fluorescence (ChlF) share the same source of energy originating from photosynthetically active radiation (PAR) absorbed by chlorophyll ($APAR_{chl}$), which can be written using a light use efficiency approach (Monteith, 1972):

$$ChlF = PAR \times fPAR_{chl} \times \phi_F \quad (1)$$

$$A_{leaf} = PAR \times fPAR_{chl} \times \phi_P \quad (2)$$

where $\phi_F$ and $\phi_P$ represent the efficiencies for ChlF emission and photochemistry, respectively. $fPAR_{chl}$, being different from the conventional definition of fraction of photosynthetically active radiation absorption, only considers the fractions absorbed by chlorophyll pigments where the photosynthesis and fluorescence originate (Zhang et al., 2018c). However, ChlF measurements have been mostly conducted at the leaf level, using pulse amplitude modulation (PAM) fluorometers (Porcar-Castell et al., 2008; Roháček and Barták, 1999). In this case, the measured ChlF intensity is not induced by the sun but by the modulated light source. Although the absolute value of the ChlF intensity does not directly link to $A_{leaf}$, it can still be used to calculate the fluorescence yield and investigate the reaction mechanism of the energy partitioning during the light reaction, and to calculate the quantum yield for photochemistry or as tool to detect plant reactions under stress (Adams and Demmig-Adams, 2004; Flexas et al., 2002).

The successful retrieval of solar-induced (steady-state) chlorophyll fluorescence (SIF) from satellites have made it possible for vegetation photosynthetic activities to be observed at the global scale (Frankenberg et al., 2011; Guanter et al., 2012; Joiner et al., 2011, 2013). Satellite SIF can be expressed as a function similar to the ChlF at the leaf level but with extra terms considering the radiative transfer within the canopy and through the atmosphere (Joiner et al., 2014):

$$SIF_{sat}(\lambda) = PAR \times fPAR_{chl} \times \Theta_F(\lambda) \times f_{esc}(\lambda, \theta_s, \theta_v, \phi) \times \tau_{atm}(\lambda, \theta_s, \theta_v, \phi) \quad (3)$$

where the satellite retrieved SIF ($SIF_{sat}$), fluorescence yield ($\Theta_F$), $f_{esc}$, $\tau_{atm}$ are all functions of the wavelength ($\lambda$), in addition, $f_{esc}$ and $\tau_{atm}$ are also affected by sun-sensor geometry characterized by sun zenith angle ($\theta_s$), view zenith angle ($\theta_v$), relative azimuth angle ($\phi$). $f_{esc}$ is a factor describing how much SIF emitted by the chloroplast leaves the canopy, and $\tau_{atm}$ is a function of atmospheric optical depth, which indicates how much SIF that leaves the canopy top passes through the atmosphere before it is captured by the satellite sensors. It should be noted that the fraction of PAR for fluorescence ($fPAR_F$)

may have different activation spectrum than that for photosynthesis ($fPAR_{chl}$), but this difference is ignored here for simplicity. Although additional factors come into play during this process, satellite retrieved SIF shows high consistency with GPP using both model simulations and ground-based measurements from eddy covariance (EC) flux towers, at least at the monthly time scale (Guanter et al., 2014; Li et al., 2018a; Zhang et al., 2016c, 2016b). In addition, recent studies suggest that the GPP-SIF relationship is consistent across biome types (Sun et al., 2017). This finding, if valid across all biomes, would greatly benefit the usage of SIF for model benchmarking (Luo et al., 2012) and global GPP estimation.

However, several issues hinder exploring the relationship between SIF and *in situ* GPP estimates. Since the SIF signal is very small and sensors used to retrieve SIF were not initially built to estimate SIF, the satellite-retrieved SIF usually has a large footprint and large uncertainties in individual retrievals (Frankenberg et al., 2014; Joiner et al., 2013, 2016). For instance, the SIF retrieval from Global Ozone Monitoring Experiment-2 (GOME-2) has a footprint of 40 km×40 km or larger; and the SIF from Greenhouse gases Observing SATellite (GOSAT) has a circular footprint with 10.5 km in diameter. Direct comparison between the satellite retrieved SIF signal and GPP estimates from EC flux tower sites thus faces the problem of spatial inconsistency except in areas of large homogenous landscape, e.g., the US Midwest cropland (Zhang et al., 2014) or boreal evergreen forests (Walther et al., 2016). However, corn (C4 pathway) and soybean (C3 pathway) in SIF footprints have different electron use efficiencies (Guan et al., 2016), which should affect the relationship between SIF and GPP. The low precision of SIF measurements also leads to a need for averaging multiple pixels either in space or time before being used.

SIF retrieved from the Orbiting Carbon Observatory-2 (OCO-2) satellite partially solved this issue with a much smaller footprint size (1.3 km×2.25 km), higher signal to noise ratio compared to GOSAT (relatively higher SIF retrieval accuracy) and much larger numbers of observations per day (Frankenberg et al., 2014; Sun et al., 2018). However, due to the sparse sampling strategy and long revisit cycle, the OCO-2 SIF data have large gaps between nearby swaths and the average sampling frequency for each flux tower site is only 3.21/year during 2015-2016 (Lu et al., 2018). In addition, OCO-2 ~~can only generate~~is often aggregated to ~~a gridded~~ monthly dataset at relatively coarse spatial resolution, typically at 1° × 1°, which limits its application in small regions. Although several statistical methods have been proposed to downscale satellite observations to finer spatial-temporal resolutions (Tadić et al., 2015, 2017), considering the large land surface heterogeneity and wide gaps between OCO-2 swaths (~ 100 km), it could be challenging to apply these methods to OCO-2 SIF.

A high spatio-temporal resolution SIF dataset is needed to improve our understanding of the relationship between SIF and GPP and provide accurate GPP estimates at the global scale. As discussed previously, the satellite-observed SIF contains signals from $APAR_{chl}$, fluorescence yield, and canopy and atmospheric attenuation. $APAR_{chl}$ is considered to be the first order approximation of SIF as it exhibits high correlation with SIF at the canopy scale (Du et al., 2017; Rossini et al., 2016; Verrelst et al., 2015; Zhang et al., 2018c). Previous studies have shown that $fPAR_{chl}$ can be inversely estimated using the

surface reflectances and radiative transfer models (Zhang et al., 2005, 2016a). The canopy structure information that affects the SIF reabsorption within canopy is also embedded in the near infrared reflectance (Badgley et al., 2017; Knyazikhin et al., 2013; Yang and van der Tol, 2018). Many previous studies have shown high correlation between SIF and vegetation indices (VIs), especially VIs related to the chlorophyll concentration (Frankenberg et al., 2011; Guanter et al., 2012). Therefore, broad-band surface reflectances may have the potential to be used to estimate vegetation information and reconstruct global SIF (Duveiller and Cescatti, 2016; Gentine and Alemohammad, 2018a). However, physical models that can predict SIF (e.g. the Soil Canopy Observation, Photochemistry and Energy fluxes, SCOPE (van der Tol et al., 2009)) often require many parameters, making it difficult to use reflectance and modelling to predict SIF at a larger scale.

Neural networks (NN), together with many other machine learning algorithms, have been used with remote sensing datasets in the Earth sciences, especially for carbon and water fluxes estimation (Alemohammad et al., 2017; Jung et al., 2011; Tramontana et al., 2016), land cover mapping (Kussul et al., 2017; Zhu et al., 2017), soil moisture retrievals and downscaling (Alemohammad et al., 2018; Kolassa et al., 2018) or to bypass parameterization (Gentine et al., 2018). These studies mostly attempted to link the satellite signals with limited *in situ* observation or model simulations for model training, while taking advantage of the large amount of data in remote sensing observations; they applied the trained algorithm to generate a regional or global dataset. Reconstructing SIF from surface reflectance, on the other hand, uses no *in situ* observations but faces more problems related to the satellite data quality assurance. The SIF-reflectance relationship is complicated, and the NN benefits from the fact that an explicit physical and radiative transfer relationship is not required.

In this study, we aim to generate a global ~~continuous~~contiguous SIF (CSIF) product based on the SIF retrievals from OCO-2 and surface reflectances from Moderate-resolution imaging spectroradiometer (MODIS) onboard Terra and Aqua satellite. The CSIF dataset aims to fill the spatial gaps between the OCO-2 swaths and temporal gaps due to the long revisit cycle of OCO-2. Specifically, we first trained and validated the NN using the satellite observed instantaneous SIF under clear-sky conditions so that the relationship is not affected by cloud-related artifacts. We further generated two SIF products, namely the clear-sky instantaneous SIF ($CSIF_{clear\text{-}inst}$) and the all-sky daily SIF ($CSIF_{all\text{-}daily}$). The spatio-temporal variations of these CSIF products were analyzed and compared with SIF from OCO-2 and ~~two~~ three other GOME-2 SIF datasets. Finally, we showed two applications of CSIF datasets: (1) monitoring drought impact using $CSIF_{clear\text{-}inst}$ and OCO-2 SIF; (2) evaluating the GPP-SIF relationship by comparing $CSIF_{~~all\text{-}daily~~}$ with GPP estimates from 40 flux tower sites.

## 2 Materials and methods

### 2.1 OCO-2 solar-induced chlorophyll fluorescence dataset

The 8100r OCO-2 SIF data between September 2014 to December 2017 were used for NN training and evaluation (Frankenberg, 2015; Frankenberg et al., 2014; Sun et al., 2018). The daily sounding-based SIF retrievals at 757 nm were first

aggregated to 0.05-degree (around 5.6 km×5.6 km at equator), consistent with MODIS climate model grid (CMG) resolution. The reasons for using this resolution include: (1) it is directly comparable (in the same order of magnitude) to the OCO-2 SIF footprint size (around 1.3km×2.25km) and the samples within each gridcell can be more evenly distributed and, thus, more representative of the gridcell SIF values than using much coarser $1° \times 1°$ or $2° \times 2°$ grids; (2) by averaging multiple observations, the uncertainty in the SIF signal can be approximately reduced by a factor of $\sqrt{n}$ ($n$ is the number of observations within this gridcell), assuming independent estimates and homogeneous SIF value within each gridcell (Frankenberg et al., 2014). During this aggregation, we only used cloud-free observations indicated by the OCO-2 cloud flag. For each 0.05-degree gridcell, the SIF value was only calculated when it contained more than 5 cloud-free SIF soundings. Although several studies have shown that SIF at different wavelengths has different sensitivity to stress and leaf and canopy reabsorption (Porcar-Castell et al., 2014; Rossini et al., 2015, 2016), we only use SIF at 757nm since it showed superior performance than SIF at 771nm in predicting GPP (Li et al., 2018a). The years 2015 and 2016 were used for training and 2014 and 2017 were used for validation. Altogether 2947819 SIF gridcells passed quality check during 2014-2017. Figure 1 shows the spatial distribution of the SIF gridcells used for training and validation (test). It should be noted that the OCO-2 satellite starts to obtaining data from September 2014 and experienced some malfunctioning during August and September in 2017, causing lower coverage for validation samples in boreal regions.

In addition to these cloud-free observations, we also calculated the all-sky SIF at 0.05-degree resolution. All SIF retrievals that passed the suggested quality checks (documented in detailed by Sun et al. (2018)) were used for the aggregation. The aggregated all-sky instantaneous SIF retrievals were converted to daily values based on the solar zenith angle (Zhang et al., 2018a). We used this dataset to validate the all-sky daily SIF ($CSIF_{all\text{-}daily}$) (see section 2.5). In both cloud free and all-sky aggregations, only observations from the nadir mode were used since glint mode tends to underestimate SIF (Sun et al., 2018).

### 2.2 MODIS reflectance dataset (MCD43C4 V006)

We used the 0.05-degree daily Nadir Bidirectional reflectance distribution Adjust Reflectance (NBAR) product from MODIS (MCD43C4 V006) during 2000-2017 as input variables for the NN. The NBAR product compute the reflectance at a nadir viewing angle for each pixel at local solar noon. Compared to MOD09 or MYD09 surface reflectance product, it removed the angle effects, and therefore, should be more stable and consistent (Schaaf et al., 2002). This dataset was processed in two different ways for training and prediction. For the training process, following (Gentine and Alemohammad, 2018a), we extracted the reflectance from the first four bands of MODIS (centered at 645nm, 858nm, 469nm and 555nm, respectively) for the corresponding pixels and days ~~with~~ when the cloud-free SIF observations were obtained. It should be noted that although the MCD43C4 is generated for each day and can match the daily SIF observations, the MCD43C4 NBAR uses 16-day worth of inputs and so that the reflectances includes the information of other days than the day of interest. However, we consider this to have limited effects since: (1) the vegetation growth/changes are continuous in time,

(2) the NBAR product uses 16-day of data but also emphasizes the specific day of interest (Schaaf, 2018). These four bands were selected because the visible and near-infrared band included most of the vegetation information and drives the variation of SIF (Verrelst et al., 2015). We also tested using all 7 band with/without the meteorological variables (temperature and vapor pressure deficit, obtained from the OCO-2 SIF lite files) to train the NN, but the improvement in training and validation were very minor ($R^2$ increased by less than 0.01, data not shown) and thus we decided not to use it. Since SIF is very sensitive to the incoming solar radiation, using cloud-free training samples can minimize the uncertainty of using cosine of the solar zenith angle as the proxy of incoming PAR. It should be noted that the training dataset may contain snow-affected samples, but these were not removed to get a more realistic prediction of SIF during winter.

For prediction, we first aggregated the daily reflectance to 4 days. The 4-day temporal resolution is selected to reach a balance among application requirements, information redundancy and dataset sizes. During this process, we used a gap-filling and smoothing algorithm to reconstruct the surface reflectance for the ~~seven~~ four bands. The detailed description of the gap-filling algorithm can be found in Zhang et al. (2017a). In this study, we slightly modified the algorithm by not applying the Best Index Slope Extraction (BISE) algorithm and Savitzky-Golay (SG) filter. The reconstructed 4-day 0.05-degree reflectance together with other datasets allowed us to predict SIF at 4-day 0.05-degree resolution during 2000-2017. Since this processing does not involve any extra information and only uses the reflectance observations from the successful model inversion~~best atmospheric conditions~~, it should be comparable to the reflectance used for NN training.

### 2.3 Machine learning algorithms

A feedforward neural network (NN) is a number of computational nodes (called neurons) structured in a single or multi-layer architecture. Each neuron is connected with all neurons in the previous layer and next layer. The neuron values are calculated using an activation function with a pre-activated value, i.e., the weighted sum of all neurons in previous layer plus biases. The training of the NN attempts to optimize these weights and biases so that the differences between the output variable in the training data and NN prediction is minimized. In this study, we used Tensorflow (https://www.tensorflow.org) and built feedforward networks with 1-3 layers and 2-9 neurons for each layer. After training models with data from 2015 and 2016, we validated the models using the test dataset from year 2014 and 2017. We then picked the one with best performance and simplest structure for SIF prediction. The rectified linear unit (ReLU) was used as the activation function since it has shown better performance in our application and the cost function used is the root-mean-square error (RMSE). We used 50 epochs with a batch size of 1024. Before training, each variable was normalized by its mean and standardized deviation. Since the NN is not deep and there is no sign of overfitting, we did not use any regularization methods during the training.

### 2.4 Reconstructing the clear-sky instantaneous SIF and daily SIF

During the NN training process, we only used the SIF and reflectance data in clear-sky conditions, and therefore cos(SZA) was used as a proxy of the incoming photosynthetically active radiation at top-of-canopy. In the prediction process, we also

used the calculated cos(SZA) based on the satellite overpass local solar time and latitude. Since we did not consider the cloud and aerosol attenuation of the PAR, this product was referred to as the "clear-sky instantaneous SIF ($CSIF_{clear\text{-}inst}$)".

In addition to the clear-sky instantaneous SIF, we also calculated two daily SIF data by assuming that the incoming solar radiation is the only factor that drives the diurnal cycle (Zhang et al., 2018a). All-sky daily SIF ($CSIF_{all\text{-}daily}$) can be calculated using the clear-sky top-of-canopy radiation ($PAR_{clear\text{-}inst}$) and the daily average radiation from Breathing Earth System Simulator (BESS) (Ryu et al., 2018):

$$CSIF_{all-daily} = \frac{CSIF_{clear-inst}}{PAR_{clear-inst}} \times PAR_{daily}^{BESS} \qquad (4)$$

where $PAR_{clear-inst}$ was calculated following previous studies that only considered atmospheric scattering (see Appendix A1). Clear-sky daily SIF ($CSIF_{clear\text{-}daily}$) assumes no cloud throughout the day and can be calculated by multiplying $CSIF_{clear\text{-}inst}$ with a daily correction factor ($\gamma$) (Zhang et al., 2018a):

$$CSIF_{clear-daily} = CSIF_{clear-inst} \times \gamma \qquad (5)$$

$\gamma$ is calculated as the ratio between the cos(SZA) during the satellite overpass and the daily averaged cos(SZA).

### 2.5 GOME-2 SIF ($SIF_{GOME\text{-}2}$), ~~and~~ Reconstructed SIF from GOME-2 ($RSIF_{GOME\text{-}2}$) and SIF* datasets.

In this study, we also used the GOME-2 SIF ($SIF_{GOME\text{-}2}$), ~~and~~ reconstructed SIF from GOME-2 ($RSIF_{GOME\text{-}2}$) using machine learning and SIF* dataset in comparison with our ~~continuous~~contiguous SIF from OCO-2. The GOME-2 SIF V27 was retrieved using a principle component analysis algorithm in the wavelength range 734-758 nm (Joiner et al., 2013, 2016). The V27 version, compared to the widely used V26, provides daily correction factor and improved bias correction and calibration (https://avdc.gsfc.nasa.gov/pub/data/satellite/MetOp/GOME_F/). The level 3 monthly 0.5-degree daily-average-SIF was used to compare with $CSIF_{all\text{-}daily}$.

$RSIF_{GOME\text{-}2}$ (Gentine and Alemohammad, 2018a) uses a similar machine learning technique approach to CSIF but the training is based on the bi-weekly gridded SIF product from GOME-2, and 8-day MYD09A1 reflectance dataset. Both clear-sky and cloudy-sky SIF are used for NN training. This dataset has a spatial resolution of 0.05-degree and 8-day temporal resolution. Both $RSIF_{GOME\text{-}2}$ and $CSIF_{all\text{-}daily}$ were aggregated to the 0.5-degree and semi-month to facilitate the comparison.

SIF* dataset (Duveiller and Cescatti, 2016) applies a statistical method and calibrates a model that links monthly 0.5-degree SIF to NDVI, evapotranspiration (ET) and land surface temperature (LST) dataset for each moving window. The model and its spatio-temporally varied parameters were then applied to finer resolution dataset (NDVI, ET, LST) with a weighted average to generate SIF at 0.05-degree resolution. In this study, we used the 0.5-degree monthly SIF* dataset during 2007-2013 to compare with CSIF.

### 2.6 Comparing CSIF with GPP at flux tower sites

We further compared the CSIF dataset to GPP estimates from the Tier 1 FLUXNET2015 datasets (http://fluxnet.fluxdata.org) to investigate the SIF-GPP relationship. Since the CSIF dataset is continuous in space and time, it provides many more samples pairs compared to the original OCO-2 SIF data (Lu et al., 2018). However, because of the landscape heterogeneity and inconsistency between the flux tower footprint and CSIF pixel size, a rigorous site selection is needed. We took the vegetation growth condition into consideration during this process: (1) the annual average, minimum, maximum and seasonal variability (represented by standard deviation) of normalized difference vegetation index (NDVI, from MOD13Q1 C6) for the target pixel (where the flux tower locates, 250 m by 250 m) need to be similar (within 20% difference or 0.05 NDVI) with the neighboring (5 km by 5 km) area; (2) Maximum NDVI value for target pixel and neighboring area need to greater than 0.2 (not barren). The daily GPP estimates, estimated using nighttime method (Reichstein et al., 2005) were averaged and aggregated into 4-day values to compare with CSIF. 4-day GPP based on more than 80% of half-hourly valid (not gap-filled) net ecosystem exchange was ~~removed~~retained. Only sites that have at least 92 valid observations (1 year) were used. Only 40 out of 166 sites passed these criterions and were grouped into different biome types (Table S1). In addition to $CSIF_{all\text{-}daily}$, we also calculated $CSIF_{clear\text{-}daily}$ and $CSIF_{site}$ which used flux tower observed radiation instead of $PAR_{daily}^{BESS}$ in Eq. (4).

## 3 Results

### 3.1 NN training and validation

The NN with one layer and ~~seven~~ five neurons generally predicts the OCO-2 SIF during the training with a coefficient of determination ($R^2$) around 0.8, and an RMSE of 0.18 mW $m^{-2}$ $nm^{-1}$ $sr^{-1}$ (Figure 2). The model also performs well in the validation ($R^2$=0.79, RMSE=0.18) and does not show effects of overfitting. Using a variety of layer (1-3) and neurons (2-9) combinations, we found that 1-layer with 5-neurons exhibited slightly higher model performance during the validation compared with more complex NN (Figure A1). Therefore, we chose to use the 4-band reflectances to feed the one-layer-five-neuron NN to generate the ~~continuous~~contiguous SIF for 2000 to 2017 when MCD43C4 NBAR dataset is available.

We also investigated the bias of our prediction among different biome types in Figure 3. For 9 out of 14 biome types, the differences between the $CSIF_{clear\text{-}inst}$ and the satellite-retrieved SIF are less than 10%; and most of the biases were within 5%. Wetlands and urban ecosystem show a 15% bias compared to the satellite retrieved SIF, which may be caused by the water or built-up contamination on the reflectance signal and the relatively small sample numbers. For savannas and grassland, the changes in fluorescence yield due to seasonal drought may be important, which cannot be considered in the NN based on reflectances only. Over croplands, CSIF exhibits a 12% underestimation. The croplands usually have high nitrogen/chlorophyll concentration that may not be fully captured by the four broad-band reflectances (Wu et al., 2008). Because we did not build biome-specific NNs for the training, we do not expect biome-specific (especially needle leaf vs.

broad leaf) relationships between SIF and reflectance. Interestingly, we still reproduced SIF with very high accuracy regardless of the plant function traits (PFT), i.e., leaf types and canopy characteristics (leaf clumping, etc.). This suggests that the escape factor and long-term changes in mean fluorescence yield might be correctly accounted for by the NN across PFTs, through the information available in the reflectances only. However, it should be noted that this does not suggest that the NN and reflectances can fully replicate the fluorescence yield variations due to short-term variations caused by stresses.

We also compared the times series of predicted CSIF and OCO-2 SIF for 12 typical biome types (Figure 4). The predicted CSIF accurately captures the seasonal and interannual variation for most biome types, while the standard deviation for each DOY is usually smaller than OCO-2 SIF. This may suggest that the uncertainty of SIF is smaller in CSIF dataset. For some ecosystems, e.g., DBF, MF, and CRO, CSIF shows slight underestimation during the peak growing season.

When comparing the daily average SIF from satellite retrievals with the predicted all-sky daily CSIF ($CSIF_{all\text{-}daily}$) dataset (Figure 45), the predicted SIF exhibits ~7% underestimation, with an $R^2$ of 0.71 and a RMSE of 0.08 mW $m^{-2}$ $nm^{-1}$ $sr^{-1}$. The clear-sky daily CSIF ($CSIF_{clear\text{-}daily}$) shows ~11% overestimation, with a slightly higher $R^2$ and lower RSME. Considering the uncertainty in SIF retrievals and the inconsistency in time of the comparison (satellite SIF was based on instantaneous PAR at the time of satellite overpass and converted to daily values assuming the atmospheric condition did not change within a day, predicted CSIF was based on 4-day average PAR), the all-sky daily CSIF performs reasonably well.

### 3.2 Spatial temporal variation of the global 0.05-degree SIF datasets

Using the trained NN with the gap-filled reflectance datasets, we produced two global CSIF datasets at 4-day temporal and 0.05-degree spatial resolution. Figure 5 6 shows the spatial patterns of the 90 percentile for each pixel and the annual average for both clear-sky instantaneous CSIF ($CSIF_{clear\text{-}inst}$) and the all-sky daily average CSIF ($CSIF_{all\text{-}daily}$). For the 90 percentile, $CSIF_{clear\text{-}inst}$ exhibits hotspots in the tropical rainforest, south Asia, and North America Corn belt, consistent with regions with high peak productivity (Guanter et al., 2014); $CSIF_{all\text{-}daily}$ shows similar spatial patterns, but with relatively lower values in the tropical forest, due to the persistent cloud coverage. For the annual average SIF, tropical forests exceed temperate cropland and show very high values for instantaneous clear-sky SIF. In all conditions, African tropical forests exhibit lower values than Amazon and Southeast Asia tropical forests.

We further investigated the seasonal and interannual variation of the all-sky daily SIF across the latitudes. The tropical regions show continuous high SIF values across seasons and the northern mid- to high-latitude regions also exhibit recurrent high values during the northern hemisphere summers (Figure 6a7a). Near 40°S a hot spot is present in austral Summer, with high interannual variability. Low SIF values can be found in dry years (2006-2007, 2009-2010) while high values were observed in wet or normal years (20102010-2011, 2012-20142015). The global average SIF also displays a strong seasonality coinciding with the North Hemisphere growing season (Figure 6b7b). For the annual total SIF values, a

statistically significant increasing trend (Mann-Kendall test, $p$<1e-4) is found with around 0.39% increase per year. Year 2015 exhibited a low anomaly after detrending, which may be caused by the El Niño events (Figure ~~6e~~7c).

The spatial pattern of the trend in $CSIF_{all\text{-}daily}$ is displayed in Figure ~~7~~8. Increasing trend dominates Europe, southeast Asia and south Amazon. Decreasing trend is mostly found in east Brazil, east Africa and some area inland Eurasia. The histogram also shows a positive shift with a magnitude (0.00027 mW $nm^{-1}$ $sr^{-1}$ $yr^{-1}$) similar to the average global trend in Figure ~~6e~~7c. The spatial pattern of $CSIF_{all\text{-}daily}$ is very similar with the trend pattern of MODIS EVI (C6) (Zhang et al., 2017b), but the south Brazilian Amazon forest shows a more positive trend than that of EVI.

### 3.3 Comparison between SIF from GOME-2 and CSIF

We then compared the CSIF datasets with the reconstructed SIF (RSIF) and SIF* based on coarser-scale and all-sky GOME-2. Although these ~~two~~ datasets were trained based on different satellites, ~~and different surface reflectance datasets were used to predict SIF,~~ the relationship between CSIF and RSIF or CSIF and SIF* is consistent across most regions ~~of~~ across the globe (Figure ~~8~~9). The $R^2$ values are generally high (> 0.8) for most regions except over tropical rainforests, barren regions in western US, northwestern China and northern Canada and Russia. The low $R^2$ values are mostly due to the relatively low variability in the temporal domain in the tropics but are also indicative of regions strongly polluted by cloud cover in which CSIF might have a competitive advantage, as the training OCO-2 data better observes the surface due to smaller footprint and with higher signal to noise ratio. The regression slopes ~~exhibit~~ are higher for ~~more productive~~ regions with persistent cloud cover (e.g., tropical forest~~, US Midwest, temperate Eurasia~~). In the time series comparison (Figure 9e-p), all three SIF datasets show similar seasonal patterns, while GOME-2 based RSIF and SIF* generally show higher values than CSIF. In addition, RSIF exhibits larger fluctuation during the non-growing season for some sites, which may be caused by snow contamination.

We further compared the $CSIF_{all\text{-}daily}$ with GOME-2 daily average SIF (Figure ~~9~~10). In general, the correlation is much lower as compared with RSIF for most regions. For regions with high variability in temporal domain, the $CSIF_{all\text{-}daily}$ still shows high $R^2$ values with respect to GOME-2 SIF. The regression slopes exhibit smaller variation except for the Amazonian tropical rainforests, southeast Asia, and barren regions in Sahara, western US, northwestern China, central Australia and Andes mountains in South America. In general, considering the various uncertainties and different satellite overpass times, sensors used, and retrieval algorithms, $CSIF_{all\text{-}daily}$ well captured the GOME-2 SIF variations both in space and time. In addition, since GOME-2 SIF in most Argentina is affected by the South American Anomaly (SAA), the coefficient of determination values are also lower as compared with Figure 9.

### 3.4 Using CSIF for drought monitoring

Since the CSIF dataset only uses broadband reflectances, it should not contain the $SIF_{yield}$ information. Compared to the SIF retrieved from OCO-2, the difference can be mostly attributed to the $SIF_{yield}$. Therefore, the difference or ratio between $SIF_{OCO-2}$ and CSIF can reflect the environmental stress on $SIF_{yield}$. Figure ~~10~~ 11 shows the difference between instantaneous clear-day OCO-2 SIF and $CSIF_{clear\text{-}inst}$. Except for Figure ~~10c~~11c, the difference mostly captures the physiological limitation of drought on energy partitioning after being absorbed by chlorophyll. The spatial extent of drought is also well-captured by the difference, where the most severe drought impacted places also exhibited the largest decline (e.g., Namibia, Botswana, Zimbabwe in (a), northeast Amazon in (b) and southern Spain, south most France, central Italy, Croatia and Bosnia and Herzegovina). The drought impact on California is less pronounced, possibly because of the irrigation systems and sparse sampling points.

We further focused on the 2015 European drought to compare the drought response of CSIF and two vegetation indices (normalized difference vegetation index, NDVI; enhanced vegetation index, EVI). Because the OCO-2 samples were not collected at the same swath for each DOY, a large fluctuation can be found in OCO-2 SIF and on the CSIF (which are using the same pixels for a fair comparison) (Figure ~~11a~~12a-d). However, when calculating the ratio between CSIF and OCO-2 SIF, its variation can be mostly attributed to the variation in $SIF_{yield}$, which can quantify the drought stress on plant physiology. In all three regions, the ratio between OCO-2 SIF and CSIF experienced a decrease during the drought period, but the signal is only obvious after applying a smoothing filter. The two vegetation indices, NDVI and EVI, on the other hand, show a reduced response in Spain and Italy, perhaps due to the plants adaption or very short drought duration.

### 3.5 GPP-CSIF relationship across biome types

With this ~~continuous~~ contiguous $SIF_{all\text{-}daily}$ dataset, we finally evaluated the GPP-CSIF relationship using GPP estimates from 40 flux tower sites from FLUXNET tier 1 dataset. The regression slope between GPP and CSIF ($a_{GPP/CSIF}$) spreads across sites with a regression slope ranging from 11.91 to 68.59 (g C $m^{-2}$ $day^{-1}$/mW $m^{-2}$ $nm^{-1}$ $sr^{-1}$) for $CSIF_{all\text{-}daily}$, 11.61 to 72.10 (g C $m^{-2}$ $day^{-1}$/mW $m^{-2}$ $nm^{-1}$ $sr^{-1}$) for $CSIF_{site}$ and 11.37 to 62.75 ~~11.61 to 72.10~~ (g C $m^{-2}$ $day^{-1}$/mW $m^{-2}$ $nm^{-1}$ $sr^{-1}$) for $CSIF_{clear\text{-}daily}$. The $R^2$ value for each individual site ranges from 0.01 to 0.93 with a median value of 0.64, 0.62 and 0.69 for all-daily, site, and clear-daily CSIF, respectively. The RMSE is 1.67 g C $m^{-2}$ $day^{-1}$ on average.

Although the CSIF-GPP relationship varies across 40 sites, when lumping all observations within each biome type, the variation is smaller (c.v. = 0.16, rhombus in Figure ~~12~~ 13c,f,i). Specifically, ENF exhibited a significant larger $a_{GPP/CSIF}$ (two-tiled student's t test, p=0.036), which is caused by a stronger canopy reabsorption/scattering of SIF. OSH only have one site and also showed very high value. If both biomes are eliminated, the $a_{GPP/CSIF}$ for rest biomes exhibited smaller variation (c.v. = 0.08).

The CSIF-GPP relationship not only varies across biome, but also varies within each biome type, especially for evergreen needleleaf forest (ENF, 9 sites), grassland (GRA, 8 sites) and wetland (WET, 2 sites) (Figure ~~12~~ 13c,f). For $CSIF_{all\text{-}daily}$, the average within-biome variation of $a_{GPP/CSIF}$ (c.v. = 0.26±0.08) is comparable to cross-sites variations (c.v. = 0.34), but larger than the cross-biome variations (c.v. = 0.16, using the biome-specific CSIF-GPP factor). Similar pattern can be found using $CSIF_{site}$ or $CSIF_{clear\text{-}daily}$.

## 4 Discussion

### 4.1 Information in ~~continuous~~contiguous SIF produced by machine learning

Vegetation photosynthetic activity has variations in several respects controlled by vegetation type, phenology, coverage, and interactions with the environment. These variations can be expressed in the spatial, seasonal, diurnal and/or interannual domains (Zhang et al., 2018a). Machine learning algorithms, try to minimize the differences between the predicted SIF and the satellite observed SIF. For OCO-2 SIF and the MODIS reflectance used for NN training, the variance in the spatial and seasonal domains are largest. Therefore, the NN generally predicts SIF well in these two domains. The interannual variations (i.e., the variations caused by year to year anomalies, e.g. due to drought) typically have much smaller variance and is more difficult to capture. This is why some machine learning products fail to reproduce interannual variability accurately (Jung et al., 2011). Using additional variables that is sensitive to this interannual anomaly in the model training can improve the model performance (Alemohammad et al., 2017; Gentine and Alemohammad, 2018b; Tramontana et al., 2016).

In this study, since the variations in $SIF_{yield}$ are relatively small (Lee et al., 2015), and cannot be detected by broadband surface reflectances, the $SIF_{yield}$ information may not be reproduced by our CSIF data. Because the environmental limitation on $SIF_{yield}$ may be complicated (may not be a linear combination of temperature, VPD or surface reflectance in the shortwave infrared) and biome specific (van der Tol et al., 2014), inclusion of other environmental variables and reflectances in shortwave bands during NN training did not greatly increase the SIF prediction accuracy. It should also be noted that $SIF_{yield}$ is relatively stable when no strong environmental limitation is present (Zhang et al., 2018c). Therefore, the CSIF product should be considered as a good proxy of OCO-2 SIF.

The satellite-retrieved SIF has a relatively large uncertainty for each individual sounding, typically ranging between 0.3-0.5 mW $m^{-2}$ $nm^{-1}$ $sr^{-1}$ (Frankenberg et al., 2014). Previous site-level studies usually use SIF averaged over a large buffered area (Li et al., 2018a; Verma et al., 2017) to reduce the uncertainty. Assuming the uncertainty is unbiased and has a Gaussian distribution, machine learning algorithms are designed to reproduce SIF with lower uncertainty. Compared with previous

studies that use light use efficiency models to downscale SIF to higher resolution (Duveiller and Cescatti, 2016), this study does not rely on multiple modeled input (evapotranspiration for example) that may introduce additional uncertainties.

We also found a significant increasing trend (0.39% year$^{-1}$) in the global annual $CSIF_{all\text{-}daily}$ (Figure ~~6~~7). This trend is close to the GPP trend derived from the satellite-data driven vegetation photosynthesis model (VPM) (0.32% year$^{-1}$) (Zhang et al., 2017a), but much greater than GPP derived from other remote sensing data-driven models (FluxCOM 0.01% year$^{-1}$ (Tramontana et al., 2016), BESS GPP 0.22% year$^{-1}$ (Jiang and Ryu, 2016), MODIS C6 0.26% year$^{-1}$ (Zhao et al., 2005), and WECANN -0.8% year$^{-1}$ [affected by the decreasing GOME-2 SIF trend (Zhang et al., 2018b)] (Alemohammad et al., 2017)). Considering there is no significant trend (-0.02% year$^{-1}$, $p$>0.1) in BESS PAR (Ryu et al., 2018), this increase is likely caused by the greening of the Earth (Zhang et al., 2017b; Zhu et al., 2016) as captured in the MODIS reflectance data. This increasing trend is also within the range of most Earth system models' predictions (Anav et al., 2015). We also observed a more pronounced increasing trend in southern Amazon than using MODIS EVI (Zhang et al., 2017b). This may suggest that CSIF is less likely to suffer from high biomass saturation than optical vegetation indices and can more effectively detect changes in tropical rainforests or over high leaf area regions such as croplands.

### 4.2 The use of satellite SIF for drought monitoring

Drought can be categorized into different stages. At an early stage, when plants sense water deficit in the soil and higher vapor pressure deficit in the atmosphere, they reduce water loss through stomatal closure. This, in turn, also reduces the $CO_2$ exchange from stomatal closure and inhibits photosynthesis. The quantum yield for heat dissipation will increase accompanied with a decrease in quantum yield for photochemical quenching and fluorescence (Genty et al., 1989; Porcar-Castell et al., 2014). This should allow satellites to potentially capture this decrease in the SIF signal (especially during the mid-noon when stress is more pronounced) as an indicator of vegetation stress. In the second stage, with prolonged dry conditions, plants will recycle the nitrogen in the leaves as represented by a decrease of the greenness (chlorophyll content) of leaves. In the third stage, if the drought continues, leaf senescence and vegetation mortality may follow. SIF can potentially detect changes during all those drought stages, whereas broadband reflectances based indices (NDVI, EVI) should only see the second and third stages.

Previous drought monitoring studies have mostly used vegetation indices (VIs) as a indictor of drought stress (Ji and Peters, 2003; Zhang et al., 2013). However, vegetation indices can only respond to drought changes in the plants' optical properties (mostly during the second and third stages). For most plants, there might be a tipping point where plants will not recover from drought-induced xylem cavitation (Urli et al., 2013). Since most VIs (e.g., NDVI, EVI) are most sensitive to the canopy changes, drought monitoring based on VIs may not be useful for drought mitigation and agricultural irrigation management. SIF retrievals from satellite, comparing with optical reflectance signals, carries the information not only about the PAR absorption by chlorophyll, but also about the drought stress on plant physiology. Although previous studies used satellite-

based SIF dataset for post-drought impact assessment (Lee et al., 2013; Yoshida et al., 2015; Sun et al., 2015; Wang et al., 2016), these studies did not separate the contribution of decreased $APAR_{chl}$ or deceased $SIF_{yield}$. A more recent study compared the SIF and VIs in India during a heat stress (Song et al., 2018), and found that SIF is more sensitive to heat stress than VIs. Similarly, since NDVI and EVI cannot well capture the change in chlorophyll concentration, heat stress on $APAR_{chl}$ and $SIF_{yield}$ cannot be fully separated. This study developed a new method to compare the difference between SIF signals and the reflectances, which can be applied for early drought warning at global scale. Although daily OCO-2 data has large gaps between swaths, combining several days observation can provide enough spatial coverage considering the spatial extent for most drought events. The spatial coverage issues could be further improved using geostatistical based methods (Tadić et al., 2017), but this may need further investigation. Comparing with other meteorological drought indices, this drought monitoring technique uses only near real-time data and avoids the inter-annual anomalies caused by other factors (land cover change, crop rotation, etc.). MCD43C4 dataset uses 16 days of inputs for the model inversion, although this may lead to temporal inconsistencies for the comparison between CSIF and OCO-2 SIF, it may have limited effect due to the higher data quality during drought because of the reduced cloud coverage.

### 4.3 Cross-biome and within-biome GPP-CSIF relationship

In contrast to Sun et al. (2017), we found a large variation of GPP-CSIF relationship across sites. Compared to previous studies, our study gave higher $a_{GPP/CSIF}$ estimates, probably due to a much higher $a_{GPP/CSIF}$ value for evergreen needleleaf forest (10 out of 40 sites are ENF) (Tables S1) and slight underestimation of $CSIF_{all\text{-}daily}$ dataset. This higher $a_{GPP/CSIF}$ value for ENF was also suggested by the comparison between OCO-2 SIF and FluxCom GPP dataset (Sun et al., 2018) and other comparisons using GOSAT SIF (Guanter et al., 2012). In consistent with (Li et al., 2018b), we also found small cross-biome variation of GPP-SIF relationship. However, a large within-biome variation of $a_{GPP/CSIF}$ is also found, which contributes to a large proportion of the observed cross-sites variations rather than the cross-biome variation. Compared to studies that uses OCO-SIF within a large buffering area (e.g. 40km diameter circle in Verma et al. (2017)), we made the comparison over a much smaller area and much higher temporal frequency.

There are several explanations for the observed site-specific GPP-SIF relationship: (1) Leaf morphology may directly affect the reabsorption and scattering of SIF that leaves the foliage (Atherton et al., 2017), however, this factor is not considered in current SIF modeling (van der Tol et al., 2009; Verrelst et al., 2015) and will directly affect the model simulation of GPP-SIF relationship at the ecosystem scale (Verrelst et al., 2016; Zhang et al., 2016c). (2) Vegetation canopy characteristics also affect the reabsorption and scattering of SIF before leaving the canopy (Romero et al., 2018; Yang and van der Tol, 2018). (3) Atmospheric condition may attenuate and bias satellite SIF retrievals to some extent, but this effect is assumed to be small unless thick clouds are present (Frankenberg and Berry, 2017). (4) SIF and GPP likely have different sensitivities to environmental stresses (Flexas et al., 2002), therefore, ecosystems with frequent environmental stresses (e.g., drought)

during the growing season tend to have relatively lower GPP to SIF ratio. (5) Since light saturations have less effect on SIF than GPP (Damm et al., 2015; Zhang et al., 2016c), the growing-season averaged light intensity (affected by latitude, average cloud coverage), vegetation canopy structure and leaf characteristic that relates to the light saturation will also affect GPP-SIF relationship. For example, the evergreen needleleaf forests have much higher specific leaf area and usually lower sun zenith angle, making them less prone to light saturation. These factors may vary not only across biomes, but also across sites. Therefore, within one biome type, the GPP-SIF relationship can also be different.

It is also noteworthy that clear-sky daily SIF exhibited stronger correlation with GPP (Figure ~~12~~13), ~~this may be caused by the fact~~a possible explanation would be that the light use efficiency increases with diffused radiation, which partly compensates for the decrease in incoming PAR when cloud presents (Gu et al., 2002; Turner et al., 2006). Because satellite SIF retrieval algorithm discarded observations that were affected by thick cloud (Sun et al., 2018), the SIF retrievals from OCO-2 ~~tend to overestimate actual~~is positively biased than the actual SIF emission of the plants. However, ~~this overestimation corresponds to period with a higher LUE~~during periods when thick cloud are present, the LUE also increases and so does the GPP/SIF ratio. The positive SIF retrieval biases compensated the increase in GPP/SIF ratio, and therefore, contributed to a stronger correlation between satellite retrieved SIF (rather than the actual SIF emission) and GPP. ~~In other words, the satellite-retrieved SIF, rather than the actual SIF emission by the plants, may be more closely related to vegetation photosynthesis.~~

### 4.4 Uncertainties and caveats

Although our $CSIF_{clear\text{-}inst}$ showed good performance as supported by the comparison with the clear-sky instantaneous SIF retrievals from OCO-2, the $CSIF_{all\text{-}daily}$ exhibits a slight underestimation. A possible explanation is that most SIF retrievals during overcast conditions did not pass the quality checks, such that OCO-2 SIF are more likely obtained during clear-sky conditions. This is supported by the fact that if we compare OCO-2 SIF with clear-daily SIF, the $R^2$ is even higher (Figure ~~5~~6).

The canopy structure and sun-sensor geometry were not explicitly considered in our modeling and only implicitly embedded in the machine learning retrieval. Several recent studies suggest that canopy structure will affect the PAR absorption and re-absorption of SIF before leaving the canopy ($f_{esc}$ in equation 3) (Knyazikhin et al., 2013; Liu et al., 2016; Yang and van der Tol, 2018), and further affect the GPP-SIF relationship (He et al., 2017; Migliavacca et al., 2017; Zhang et al., 2016c). However, most of these studies made assumptions requiring either a dense canopy or non-reflecting soil and thus cannot be easily applied at the global scale. In addition, OCO-2 SIF data used in this study are from nadir observations, while both the MODIS and GOME-2 sensors acquire images both nadir and near nadir. Such discrepancy in observation angles may induce bidirectional effects. Since CSIF is trained based on the satellite observed SIF instead of the canopy SIF emission, and as

previously discussed, it did not consider the atmospheric attenuation of SIF signal in the presence of clouds. The CSIF values are expected to be closer to the canopy SIF emission than the satellite-observed SIF at top-of-atmosphere.

The BESS PAR 4-day dataset has high overall accuracy (RRMSE=15.2%) and very little bias (1.4%). For different climate zones, the uncertainties are typically under 20%. These uncertainties do not affect the $CSIF_{clear\text{-}inst}$ data but will propagate to $CSIF_{all\text{-}daily}$.

## 5 Conclusion

In this study, using the surface reflectance from the ~~Aqua~~ MODIS instrument and a NN algorithm, we developed two spatially ~~continuous~~contiguous and high temporal resolution SIF datasets (CSIF). These two SIF products not only show high accuracy when validated against the satellite retrieved OCO-2 SIF, but also exhibit reasonably high consistency with both reconstructed and satellite retrieved GOME-2 SIF. $CSIF_{all\text{-}daily}$ exhibits an increasing trend globally during 2001-2016, which is attributed to the Earth greening and not to changes in PAR. Since the CSIF dataset include most information of PAR absorption of chlorophyll, the difference between OCO-2 SIF and CSIF mostly contains the information of physiological stress on fluorescence yield. This indicator is found to be effective for early drought warning than vegetation indices. By comparing $CSIF_{all\text{-}daily}$ with GPP estimates across 40 EC flux tower sites, the GPP-SIF relationship is found to vary across sites, and a large proportion of this comes from within-biome variation. However, this finding still requires further examination using SIF from both new satellites instruments (e.g., TROPOMI) and ground-based measurements. The high resolution CSIF dataset can be further used for regional to global carbon and water fluxes analysis.

**Code availability:**

The code used to generate the CSIF dataset is available at https://github.com/zhangyaonju/continous_SIF.

**Data availability:**

The CSIF dataset ($CSIF_{clear\text{-}inst}$, $CSIF_{clear\text{-}daily}$ and $CSIF_{all\text{-}daily}$) with a 0.5-degree spatial resolution and 4-day temporal resolution can be access through Figshare: DOI:10.6084/m9.figshare.6387494. The 0.05-degree 4-day dataset can be obtained upon request, given the large size. The MCD43C4 dataset can be access through NASA EARTHDATA (https://earthdata.nasa.gov). The BESS PAR product can be access through Environmental Ecology Lab at Seoul National University (http://environment.snu.ac.kr/bess_rad/).

## Appendix

### A1. Calculation of clear-sky radiation

We calculated the clear-sky radiation following previous studies (Duffie and Beckman, 2013; Ryu et al., 2018). The total surface shortwave radiation $R_T$ is the summation of direct surface ~~bean~~ beam radiation ($R_{sb}$) and diffused radiation (~~$R_{sb}$~~$R_{sd}$):

$$R_T = R_{sb} + R_{sd} \quad \text{(A1)}$$

$R_{sb}$ and $R_{s\text{~~b~~}d}$ are calculated as the product of the top of atmosphere shortwave radiation ($R_{TOA}$) and the atmospheric transmittance for beam radiation ($\tau_b$) and that for diffused radiation ($\tau_d$):

$$R_{sb} = R_{TOA} \times \tau_b \quad \text{(A2)}$$

$$R_{sd} = R_{TOA} \times \tau_d \quad \text{(A3)}$$

where $R_{TOA}$ is calculate as a function of solar constant ($S_0$=1360.8 W m$^{-2}$), the proportion of solar irradiance within shortwave range ($\alpha$=0.98), the day of year ($n$) and the cosine of the solar zenith angle ($\cos\theta_s$):

$$R_{TOA} = S_0 \times \alpha \times \left[1 + 0.033\cos\left(\frac{2\pi n}{365}\right)\right] \times \cos\theta_s \quad \text{(A4)}$$

And $\tau_b$ is calculated as:

$$\tau_b = a_0 + a_1 \exp\left(\frac{-k}{\cos\theta_s}\right) \quad \text{(A5)}$$

where $a_0$, $a_1$, and $k$ are coefficients that consider the atmospheric attenuation based on the atmosphere path length and abundance of the gases or particles that need to be adjusted for elevation:

$$a_0 = 0.4237 - 0.00821(6 - A)^2 \quad \text{(A6a)}$$

$$a_1 = 0.5055 + 0.00595(6.5 - A)^2 \quad \text{(A6b)}$$

$$k = 0.2711 + 0.01858(2.5 - A)^2 \quad \text{(A6c)}$$

where $A$ is the elevation in kilometers. The ETOPO1 Global Relief Model was used to provide the elevation information. This dataset was downloaded from National Oceanic and Atmospheric Administration (https://data.nodc.noaa.gov/cgi-bin/iso?id=gov.noaa.ngdc.mgg.dem:316) and aggregated to 0.05 degree. In this study, we did not consider the variation of these parameters for different climate and latitudinal zones since those effects are less important. The transmittance for diffused radiation ($\tau_d$) is calculated as a function of $\tau_b$:

$$\tau_d = 0.271 - 0.294\tau_b \quad \text{(A7)}$$

## Author contribution

Y.Z. and P.G. designed the study. P.G. provided the Neuron Network training code. Y.Z. performed the analysis. P.G., S.H.A. and J.J. helped interpret the results. Y.Z. led the writing, with the input from all other authors. All authors discussed and commented on the results and the manuscript.

## Competing interests

The authors declare no competing interests.

## Acknowledgements

This work used eddy covariance data acquired and shared by the FLUXNET community, including these networks: AmeriFlux, AfriFlux, AsiaFlux, CarboAfrica, CarboEuropeIP, CarboItaly, CarboMont, ChinaFlux, Fluxnet-Canada, GreenGrass, ICOS, KoFlux, LBA, NECC, OzFlux-TERN, TCOS-Siberia, and USCCC. The ERA-Interim reanalysis data are provided by ECMWF and processed by LSCE. The FLUXNET eddy covariance data processing and harmonization was carried out by the European Fluxes Database Cluster, AmeriFlux Management Project, and Fluxdata project of FLUXNET, with the support of CDIAC and ICOS Ecosystem Thematic Center, and the OzFlux, ChinaFlux and AsiaFlux offices. The authors would like to thank Dr. Youngryel Ryu from Seoul National University for providing the BESS PAR dataset. The authors acknowledge funding from NASA NNH16ZDA001N-AIST, Computational Technologies: "An Assessment of Hybrid Quantum Annealing Approaches for Inferring and Assimilating Satellite Surface Flux Data into Global Land Surface Models.", as well as funding from the STR3S project supported by the Belgium Space Agency.

## References

Adams, W. W. and Demmig-Adams, B.: Chlorophyll Fluorescence as a Tool to Monitor Plant Response to the Environment, in Chlorophyll a Fluorescence, pp. 583–604, Springer, Dordrecht., 2004.

Alemohammad, S. H., Fang, B., Konings, A. G., Aires, F., Green, J. K., Kolassa, J., Miralles, D., Prigent, C. and Gentine, P.: Water, Energy, and Carbon with Artificial Neural Networks (WECANN): a statistically based estimate of global surface turbulent fluxes and gross primary productivity using solar-induced fluorescence, Biogeosciences, 14(18), 4101–4124, doi:10.5194/bg-14-4101-2017, 2017.

Alemohammad, S. H., Kolassa, J., Prigent, C., Aires, F. and Gentine, P.: Global Downscaling of Remotely-Sensed Soil Moisture using Neural Networks, Hydrol. Earth Syst. Sci. Discuss., 2018, 1–19, doi:10.5194/hess-2017-680, 2018.

Anav, A., Friedlingstein, P., Beer, C., Ciais, P., Harper, A., Jones, C., Murray-Tortarolo, G., Papale, D., Parazoo, N. C., Peylin, P., Piao, S., Sitch, S., Viovy, N., Wiltshire, A. and Zhao, M.: Spatiotemporal patterns of terrestrial gross primary production: A review, Reviews of Geophysics, 53(3), 785–818, doi:10.1002/2015RG000483, 2015.

Atherton, J., Olascoaga, B., Alonso, L. and Porcar-Castell, A.: Spatial Variation of Leaf Optical Properties in a Boreal Forest Is Influenced by Species and Light Environment, Front. Plant Sci., 8, doi:10.3389/fpls.2017.00309, 2017.

Badgley, G., Field, C. B. and Berry, J. A.: Canopy near-infrared reflectance and terrestrial photosynthesis, Science Advances, 3(3), e1602244, doi:10.1126/sciadv.1602244, 2017.

Baldocchi, D., Falge, E., Gu, L., Olson, R., Hollinger, D., Running, S., Anthoni, P., Bernhofer, C., Davis, K., Evans, R., Fuentes, J., Goldstein, A., Katul, G., Law, B., Lee, X., Malhi, Y., Meyers, T., Munger, W., Oechel, W., Paw U, K. T., Pilegaard, K., Schmid, H. P., Valentini, R., Verma, S., Vesala, T., Wilson, K. and Wofsy, S.: FLUXNET: A New Tool to Study the Temporal and Spatial Variability of Ecosystem-Scale Carbon Dioxide, Water Vapor, and Energy Flux Densities, Bull. Amer. Meteor. Soc., 82(11), 2415–2434, doi:10.1175/1520-0477(2001)082<2415:FANTTS>2.3.CO;2, 2001.

Beer, C., Reichstein, M., Tomelleri, E., Ciais, P., Jung, M., Carvalhais, N., Rodenbeck, C., Arain, M. A., Baldocchi, D., Bonan, G. B., Bondeau, A., Cescatti, A., Lasslop, G., Lindroth, A., Lomas, M., Luyssaert, S., Margolis, H., Oleson, K. W., Roupsard, O., Veenendaal, E., Viovy, N., Williams, C., Woodward, F. I. and Papale, D.: Terrestrial Gross Carbon Dioxide Uptake: Global Distribution and Covariation with Climate, Science, 329(5993), 834–838, doi:10.1126/science.1184984, 2010.

Chen, M., Rafique, R., Asrar, G. R., Bond-Lamberty, B., Ciais, P., Zhao, F., Reyer, C. P. O., Ostberg, S., Chang, J., Ito, A., Yang, J., Zeng, N., Kalnay, E., Tristram West, Leng, G., Francois, L., Munhoven, G., Henrot, A., Tian, H., Pan, S., Kazuya Nishina, Viovy, N., Morfopoulos, C., Betts, R., Schaphoff, S., Steinkamp, J. and Thomas Hickler: Regional contribution to variability and trends of global gross primary productivity, Environ. Res. Lett., 12(10), 105005, doi:10.1088/1748-9326/aa8978, 2017.

Damm, A., Guanter, L., Paul-Limoges, E., van der Tol, C., Hueni, A., Buchmann, N., Eugster, W., Ammann, C. and Schaepman, M. E.: Far-red sun-induced chlorophyll fluorescence shows ecosystem-specific relationships to gross primary production: An assessment based on observational and modeling approaches, Remote Sensing of Environment, 166, 91–105, doi:10.1016/j.rse.2015.06.004, 2015.

Du, S., Liu, L., Liu, X. and Hu, J.: Response of Canopy Solar-Induced Chlorophyll Fluorescence to the Absorbed Photosynthetically Active Radiation Absorbed by Chlorophyll, Remote Sensing, 9(9), 911, doi:10.3390/rs9090911, 2017.

Duffie, J. A. and Beckman, W. A.: Solar Engineering of Thermal Processes, John Wiley & Sons., 2013.

Duveiller, G. and Cescatti, A.: Spatially downscaling sun-induced chlorophyll fluorescence leads to an improved temporal correlation with gross primary productivity, Remote Sensing of Environment, 182, 72–89, doi:10.1016/j.rse.2016.04.027, 2016.

Flexas, J., Escalona, J. M., Evain, S., Gulías, J., Moya, I., Osmond, C. B. and Medrano, H.: Steady-state chlorophyll fluorescence (Fs) measurements as a tool to follow variations of net CO2 assimilation and stomatal conductance during water-stress in C3 plants, European Space Agency, (Special Publication) ESA SP, (527), 26–29, doi:10.1034/j.1399-3054.2002.1140209.x, 2002.

Frankenberg, C.: Solar Induced Chlorophyll Fluorescence., 2015.

Frankenberg, C. and Berry, J. A.: Solar Induced Chlorophyll Fluorescence: Origins, Relation to Photosynthesis and Retrieval, in Comprehensive Remote Sensing, pp. 143–162, Elsevier., 2017.

Frankenberg, C., Fisher, J. B., Worden, J., Badgley, G., Saatchi, S. S., Lee, J. E., Toon, G. C., Butz, A., Jung, M., Kuze, A. and Yokota, T.: New global observations of the terrestrial carbon cycle from GOSAT: Patterns of plant fluorescence with gross primary productivity, Geophysical Research Letters, 38(17), 1–6, doi:10.1029/2011GL048738, 2011.

Frankenberg, C., O'Dell, C., Berry, J., Guanter, L., Joiner, J., Köhler, P., Pollock, R. and Taylor, T. E.: Prospects for chlorophyll fluorescence remote sensing from the Orbiting Carbon Observatory-2, Remote Sensing of Environment, 147, 1–12, doi:10.1016/j.rse.2014.02.007, 2014.

Friedl, M. A., Sulla-Menashe, D., Tan, B., Schneider, A., Ramankutty, N., Sibley, A. and Huang, X.: MODIS Collection 5 global land cover: Algorithm refinements and characterization of new datasets, Remote Sensing of Environment, 114(1), 168–182, doi:10.1016/j.rse.2009.08.016, 2010.

Gentine, P. and Alemohammad, S. H.: Reconstructed Solar Induced Fluorescence: a machine-learning vegetation product based on MODIS surface reflectance to reproduce GOME-2 solar-induced fluorescence, Geophysical Research Letters, 2018a.

Gentine, P. and Alemohammad, S. H.: RSIF (Reconstructed Solar Induced Fluorescence): a machine-learning vegetation product based on MODIS surface reflectance to reproduce GOME-2 solar induced fluorescence, Geophysical Research Letters, 45(7), 3136–3146, doi:10.1002/2017GL076294, 2018b.

Gentine, P., Pritchard, M., Rasp, S., Reinaudi, G. and Yacalis, G.: Could Machine Learning Break the Convection Parameterization Deadlock?, Geophysical Research Letters, 45(11), 5742–5751, doi:10.1029/2018GL078202, 2018.

Genty, B., Briantais, J. M. and Baker, N. R.: The relationship between the quantum yield of photosynthetic electron transport and quenching of chlorophyll fluorescence, Biochimica et Biophysica Acta - General Subjects, 990(1), 87–92, doi:10.1016/S0304-4165(89)80016-9, 1989.

Gu, L., Baldocchi, D., Verma, S. B., Black, T. A., Vesala, T., Falge, E. M. and Dowty, P. R.: Advantages of diffuse radiation for terrestrial ecosystem productivity, Journal of Geophysical Research: Atmospheres, 107(D6), ACL 2–1–ACL 2–23, doi:10.1029/2001JD001242, 2002.

Guan, K., Berry, J. A., Zhang, Y., Joiner, J., Guanter, L., Badgley, G. and Lobell, D. B.: Improving the monitoring of crop productivity using spaceborne solar-induced fluorescence, Global Change Biology, 22(2), 716–726, doi:10.1111/gcb.13136, 2016.

Guanter, L., Frankenberg, C., Dudhia, A., Lewis, P. E., Gómez-Dans, J., Kuze, A., Suto, H. and Grainger, R. G.: Retrieval and global assessment of terrestrial chlorophyll fluorescence from GOSAT space measurements, Remote Sensing of Environment, 121, 236–251, doi:10.1016/j.rse.2012.02.006, 2012.

Guanter, L., Zhang, Y., Jung, M., Joiner, J., Voigt, M., Berry, J. A., Frankenberg, C., Huete, A. R., Zarco-Tejada, P., Lee, J.-E., Moran, M. S., Ponce-Campos, G., Beer, C., Camps-Valls, G., Buchmann, N., Gianelle, D., Klumpp, K., Cescatti, A., Baker, J. M. and Griffis, T. J.: Global and time-resolved monitoring of crop photosynthesis with chlorophyll fluorescence, Proceedings of the National Academy of Sciences, 111(14), E1327–E1333, doi:10.1073/pnas.1320008111, 2014.

He, L., Chen, J. M., Liu, J., Mo, G. and Joiner, J.: Angular normalization of GOME-2 Sun-induced chlorophyll fluorescence observation as a better proxy of vegetation productivity, Geophys. Res. Lett., 44(11), 2017GL073708, doi:10.1002/2017GL073708, 2017.

Ji, L. and Peters, A. J.: Assessing vegetation response to drought in the northern Great Plains using vegetation and drought indices, Remote Sensing of Environment, 87(1), 85–98, doi:10.1016/S0034-4257(03)00174-3, 2003.

Jiang, C. and Ryu, Y.: Multi-scale evaluation of global gross primary productivity and evapotranspiration products derived from Breathing Earth System Simulator (BESS), Remote Sensing of Environment, 186, 528–547, doi:10.1016/j.rse.2016.08.030, 2016.

Joiner, J., Yoshida, Y., Vasilkov, A. P., Yoshida, Y., Corp, L. A. and Middleton, E. M.: First observations of global and seasonal terrestrial chlorophyll fluorescence from space, Biogeosciences, 8(3), 637–651, doi:10.5194/bg-8-637-2011, 2011.

Joiner, J., Guanter, L., Lindstrot, R., Voigt, M., Vasilkov, A. P., Middleton, E. M., Huemmrich, K. F., Yoshida, Y. and Frankenberg, C.: Global monitoring of terrestrial chlorophyll fluorescence from moderate-spectral-resolution near-infrared satellite measurements: methodology, simulations, and application to GOME-2, Atmospheric Measurement Techniques, 6(10), 2803–2823, doi:10.5194/amt-6-2803-2013, 2013.

Joiner, J., Yoshida, Y., Vasilkov, A. P., Schaefer, K., Jung, M., Guanter, L., Zhang, Y., Garrity, S., Middleton, E. M., Huemmrich, K. F., Gu, L. and Belelli Marchesini, L.: The seasonal cycle of satellite chlorophyll fluorescence observations and its relationship to vegetation phenology and ecosystem atmosphere carbon exchange, Remote Sensing of Environment, 152, 375–391, doi:10.1016/j.rse.2014.06.022, 2014.

Joiner, J., Yoshida, Y., Guanter, L. and Middleton, E. M.: New methods for the retrieval of chlorophyll red fluorescence from hyperspectral satellite instruments: simulations and application to GOME-2 and SCIAMACHY, Atmos. Meas. Tech., 9(8), 3939–3967, doi:10.5194/amt-9-3939-2016, 2016.

Jung, M., Reichstein, M., Margolis, H. A., Cescatti, A., Richardson, A. D., Arain, M. A., Arneth, A., Bernhofer, C., Bonal, D., Chen, J., Gianelle, D., Gobron, N., Kiely, G., Kutsch, W., Lasslop, G., Law, B. E., Lindroth, A., Merbold, L., Montagnani, L., Moors, E. J., Papale, D., Sottocornola, M., Vaccari, F. and Williams, C.: Global patterns of land-atmosphere fluxes of carbon dioxide, latent heat, and sensible heat derived from eddy covariance, satellite, and meteorological observations, Journal of Geophysical Research: Biogeosciences, 116(3), 1–16, doi:10.1029/2010JG001566, 2011.

Knyazikhin, Y., Schull, M. A., Stenberg, P., Mottus, M., Rautiainen, M., Yang, Y., Marshak, A., Latorre Carmona, P., Kaufmann, R. K., Lewis, P., Disney, M. I., Vanderbilt, V., Davis, A. B., Baret, F., Jacquemoud, S., Lyapustin, A. and Myneni, R. B.: Hyperspectral remote sensing of foliar nitrogen content, Proceedings of the National Academy of Sciences, 110(3), E185–E192, doi:10.1073/pnas.1210196109, 2013.

Kolassa, J., Reichle, R. H., Liu, Q., Alemohammad, S. H., Gentine, P., Aida, K., Asanuma, J., Bircher, S., Caldwell, T., Colliander, A., Cosh, M., Holifield Collins, C., Jackson, T. J., Martínez-Fernández, J., McNairn, H., Pacheco, A., Thibeault, M. and Walker, J. P.: Estimating surface soil moisture from SMAP observations using a Neural Network technique, Remote Sensing of Environment, 204, 43–59, doi:10.1016/j.rse.2017.10.045, 2018.

Krause, G. H. and Weis, E.: Chlorophyll Fluorescence and Photosynthesis: The Basics, Annual Review of Plant Physiology and Plant Molecular Biology, 42(1), 313–349, doi:10.1146/annurev.pp.42.060191.001525, 1991.

Kussul, N., Lavreniuk, M., Skakun, S. and Shelestov, A.: Deep Learning Classification of Land Cover and Crop Types Using Remote Sensing Data, IEEE Geoscience and Remote Sensing Letters, 14(5), 778–782, doi:10.1109/LGRS.2017.2681128, 2017.

Lee, J.-E., Frankenberg, C., van der Tol, C., Berry, J. A., Guanter, L., Boyce, C. K., Fisher, J. B., Morrow, E., Worden, J. R., Asefi, S., Badgley, G. and Saatchi, S.: Forest productivity and water stress in Amazonia: observations from GOSAT

chlorophyll fluorescence, Proceedings of the Royal Society B: Biological Sciences, 280(1761), 20130171–20130171, doi:10.1098/rspb.2013.0171, 2013.

Lee, J.-E., Berry, J. A., van der Tol, C., Yang, X., Guanter, L., Damm, A., Baker, I. and Frankenberg, C.: Simulations of chlorophyll fluorescence incorporated into the Community Land Model version 4, Global Change Biology, 21(9), 3469–3477, doi:10.1111/gcb.12948, 2015.

Li, X., Xiao, J. and He, B.: Chlorophyll fluorescence observed by OCO-2 is strongly related to gross primary productivity estimated from flux towers in temperate forests, Remote Sensing of Environment, 204(Supplement C), 659–671, doi:10.1016/j.rse.2017.09.034, 2018a.

Li, X., Xiao, J., He, B., Arain, M. A., Beringer, J., Desai, A. R., Emmel, C., Hollinger, D. Y., Krasnova, A., Mammarella, I., Noe, S. M., Ortiz, P. S., Rey-Sanchez, C., Rocha, A. V. and Varlagin, A.: Solar-induced chlorophyll fluorescence is strongly correlated with terrestrial photosynthesis for a wide variety of biomes: First global analysis based on OCO-2 and flux tower observations, Global Change Biology, 0(ja), doi:10.1111/gcb.14297, 2018b.

Liu, L., Liu, X., Wang, Z. and Zhang, B.: Measurement and Analysis of Bidirectional SIF Emissions in Wheat Canopies, IEEE Transactions on Geoscience and Remote Sensing, 54(5), 2640–2651, doi:10.1109/TGRS.2015.2504089, 2016.

Lu, X., Cheng, X., Li, X. and Tang, J.: Opportunities and challenges of applications of satellite-derived sun-induced fluorescence at relatively high spatial resolution, Science of The Total Environment, 619–620, 649–653, doi:10.1016/j.scitotenv.2017.11.158, 2018.

Luo, Y. Q., Randerson, J. T., Abramowitz, G., Bacour, C., Blyth, E., Carvalhais, N., Ciais, P., Dalmonech, D., Fisher, J. B., Fisher, R., Friedlingstein, P., Hibbard, K., Hoffman, F., Huntzinger, D., Jones, C. D., Koven, C., Lawrence, D., Li, D. J., Mahecha, M., Niu, S. L., Norby, R., Piao, S. L., Qi, X., Peylin, P., Prentice, I. C., Riley, W., Reichstein, M., Schwalm, C., Wang, Y. P., Xia, J. Y., Zaehle, S. and Zhou, X. H.: A framework for benchmarking land models, Biogeosciences, 9(10), 3857–3874, doi:10.5194/bg-9-3857-2012, 2012.

Migliavacca, M., Perez-Priego, O., Rossini, M., El-Madany, T. S., Moreno, G., van der Tol, C., Rascher, U., Berninger, A., Bessenbacher, V., Burkart, A., Carrara, A., Fava, F., Guan, J. H., Hammer, T. W., Henkel, K., Juarez-Alcalde, E., Julitta, T., Kolle, O., Martín, M. P., Musavi, T., Pacheco-Labrador, J., Pérez-Burgueño, A., Wutzler, T., Zaehle, S. and Reichstein, M.: Plant functional traits and canopy structure control the relationship between photosynthetic CO2 uptake and far-red sun-induced fluorescence in a Mediterranean grassland under different nutrient availability, New Phytologist, 214(3), 1078–1091, doi:10.1111/nph.14437, 2017.

Monteith, J. L.: Solar Radiation and Productivity in Tropical Ecosystems, Journal of Applied Ecology, 9(3), 747–766, doi:10.2307/2401901, 1972.

Müller, J. N. C.: Untersuchungen über die diffusion der atmosphärischen gase und die gasausscheidung unter verschiedenen beleuchtungs-bedingungen, Jahrbucher fur Wissenschaftliche Botanik, (9), 36–49, 1874.

Porcar-Castell, A., Pfündel, E., Korhonen, J. F. J. and Juurola, E.: A new monitoring PAM fluorometer (MONI-PAM) to study the short- and long-term acclimation of photosystem II in field conditions, Photosynthesis Research, 96(2), 173–179, doi:10.1007/s11120-008-9292-3, 2008.

Porcar-Castell, A., Tyystjärvi, E., Atherton, J., Van Der Tol, C., Flexas, J., Pfündel, E. E., Moreno, J., Frankenberg, C. and Berry, J. A.: Linking chlorophyll a fluorescence to photosynthesis for remote sensing applications: Mechanisms and challenges, Journal of Experimental Botany, 65(15), 4065–4095, doi:10.1093/jxb/eru191, 2014.

Reichstein, M., Falge, E., Baldocchi, D., Papale, D., Aubinet, M., Berbigier, P., Bernhofer, C., Buchmann, N., Gilmanov, T., Granier, A., Grünwald, T., Havránková, K., Ilvesniemi, H., Janous, D., Knohl, A., Laurila, T., Lohila, A., Loustau, D., Matteucci, G., Meyers, T., Miglietta, F., Ourcival, J. M., Pumpanen, J., Rambal, S., Rotenberg, E., Sanz, M., Tenhunen, J., Seufert, G., Vaccari, F., Vesala, T., Yakir, D. and Valentini, R.: On the separation of net ecosystem exchange into assimilation and ecosystem respiration: Review and improved algorithm, Global Change Biology, 11(9), 1424–1439, doi:10.1111/j.1365-2486.2005.001002.x, 2005.

Roháček, K. and Barták, M.: Technique of the modulated chlorophyll fluorescence: Basic concepts, useful parameters, and some applications., 1999.

Romero, J. M., Cordon, G. B. and Lagorio, M. G.: Modeling re-absorption of fluorescence from the leaf to the canopy level, Remote Sensing of Environment, 204, 138–146, doi:10.1016/j.rse.2017.10.035, 2018.

Rossini, M., Nedbal, L., Guanter, L., Ač, A., Alonso, L., Burkart, A., Cogliati, S., Colombo, R., Damm, A., Drusch, M., Hanus, J., Janoutova, R., Julitta, T., Kokkalis, P., Moreno, J., Novotny, J., Panigada, C., Pinto, F., Schickling, A., Schüttemeyer, D., Zemek, F. and Rascher, U.: Red and far red Sun-induced chlorophyll fluorescence as a measure of plant photosynthesis, Geophysical Research Letters, 42(6), 1632–1639, doi:10.1002/2014GL062943, 2015.

Rossini, M., Meroni, M., Celesti, M., Cogliati, S., Julitta, T., Panigada, C., Rascher, U., van der Tol, C. and Colombo, R.: Analysis of red and far-red sun-induced chlorophyll fluorescence and their ratio in different canopies based on observed and modeled data, Remote Sensing, 8(5), doi:10.3390/rs8050412, 2016.

Ryu, Y., Jiang, C., Kobayashi, H. and Detto, M.: MODIS-derived global land products of shortwave radiation and diffuse and total photosynthetically active radiation at 5km resolution from 2000, Remote Sensing of Environment, 204(Supplement C), 812–825, doi:10.1016/j.rse.2017.09.021, 2018.

Schaaf, C.: MODIS BRDF/Albedo User Guide. [online] Available from: https://www.umb.edu/spectralmass/terra_aqua_modis/v006, 2018.

Schaaf, C. B., Gao, F., Strahler, A. H., Lucht, W., Li, X., Tsang, T., Strugnell, N. C., Zhang, X., Jin, Y., Muller, J.-P., Lewis, P., Barnsley, M., Hobson, P., Disney, M., Roberts, G., Dunderdale, M., Doll, C., d'Entremont, R. P., Hu, B., Liang, S., Privette, J. L. and Roy, D.: First operational BRDF, albedo nadir reflectance products from MODIS, Remote Sensing of Environment, 83(1–2), 135–148, doi:10.1016/S0034-4257(02)00091-3, 2002.

Schimel, D., Pavlick, R., Fisher, J. B., Asner, G. P., Saatchi, S., Townsend, P., Miller, C., Frankenberg, C., Hibbard, K. and Cox, P.: Observing terrestrial ecosystems and the carbon cycle from space, Global Change Biology, 21(5), 1762–1776, doi:10.1111/gcb.12822, 2015.

Song, L., Guanter, L., Guan, K., You, L., Huete, A., Ju, W. and Zhang, Y.: Satellite sun-induced chlorophyll fluorescence detects early response of winter wheat to heat stress in the Indian Indo-Gangetic Plains, Global Change Biology, 0(ja), doi:10.1111/gcb.14302, 2018.

Sun, Y., Fu, R., Dickinson, R., Joiner, J., Frankenberg, C., Gu, L., Xia, Y. and Fernando, N.: Drought onset mechanisms revealed by satellite solar-induced chlorophyll fluorescence: Insights from two contrasting extreme events, Journal of Geophysical Research G: Biogeosciences, 120(11), 2427–2440, doi:10.1002/2015JG003150, 2015.

Sun, Y., Frankenberg, C., Wood, J. D., Schimel, D. S., Jung, M., Guanter, L., Drewry, D. T., Verma, M., Porcar-Castell, A., Griffis, T. J., Gu, L., Magney, T. S., Köhler, P., Evans, B. and Yuen, K.: OCO-2 advances photosynthesis observation from space via solar-induced chlorophyll fluorescence, Science, 358(6360), eaam5747, doi:10.1126/science.aam5747, 2017.

Sun, Y., Frankenberg, C., Jung, M., Joiner, J., Guanter, L., Köhler, P. and Magney, T.: Overview of Solar-Induced chlorophyll Fluorescence (SIF) from the Orbiting Carbon Observatory-2: Retrieval, cross-mission comparison, and global monitoring for GPP, Remote Sensing of Environment, doi:10.1016/j.rse.2018.02.016, 2018.

Tadić, J. M., Qiu, X., Yadav, V. and Michalak, A. M.: Mapping of satellite Earth observations using moving window block kriging, Geosci. Model Dev., 8(10), 3311–3319, doi:10.5194/gmd-8-3311-2015, 2015.

Tadić, J. M., Qiu, X., Miller, S. and Michalak, A. M.: Spatio-temporal approach to moving window block kriging of satellite data v1.0, Geoscientific Model Development, 10(2), 709–720, doi:10.5194/gmd-10-709-2017, 2017.

van der Tol, C., Verhoef, W., Timmermans, J., Verhoef, A. and Su, Z.: An integrated model of soil-canopy spectral radiances, photosynthesis, fluorescence, temperature and energy balance, Biogeosciences, 6(12), 3109–3129, doi:10.5194/bg-6-3109-2009, 2009.

van der Tol, C., Berry, J. A., Campbell, P. K. E. and Rascher, U.: Models of fluorescence and photosynthesis for interpreting measurements of solar-induced chlorophyll fluorescence, Journal of Geophysical Research: Biogeosciences, 119(12), 2312–2327, doi:10.1002/2014JG002713, 2014.

Tramontana, G., Jung, M., Schwalm, C. R., Ichii, K., Camps-Valls, G., Ráduly, B., Reichstein, M., Arain, M. A., Cescatti, A., Kiely, G., Merbold, L., Serrano-Ortiz, P., Sickert, S., Wolf, S. and Papale, D.: Predicting carbon dioxide and energy fluxes across global FLUXNET sites with regression algorithms, Biogeosciences, 13(14), 4291–4313, doi:10.5194/bg-13-4291-2016, 2016.

Turner, D. P., Ritts, W. D., Styles, J. M., Yang, Z., Cohen, W. B., Law, B. E. and Thornton, P. E.: A diagnostic carbon flux model to monitor the effects of disturbance and interannual variation in climate on regional NEP, Tellus B: Chemical and Physical Meteorology, 58(5), 476–490, doi:10.1111/j.1600-0889.2006.00221.x, 2006.

Urli, M., Porté, A. J., Cochard, H., Guengant, Y., Burlett, R. and Delzon, S.: Xylem embolism threshold for catastrophic hydraulic failure in angiosperm trees, Tree Physiology, 33(7), 672–683, doi:10.1093/treephys/tpt030, 2013.

Verma, M., Schimel, D., Evans, B., Frankenberg, C., Beringer, J., Drewry, D. T., Magney, T., Marang, I., Hutley, L., Moore, C. and Eldering, A.: Effect of environmental conditions on the relationship between solar-induced fluorescence and gross primary productivity at an OzFlux grassland site, Journal of Geophysical Research: Biogeosciences, 122(3), 716–733, doi:10.1002/2016JG003580, 2017.

Verrelst, J., Rivera, J. P., van der Tol, C., Magnani, F., Mohammed, G. and Moreno, J.: Global sensitivity analysis of the SCOPE model: What drives simulated canopy-leaving sun-induced fluorescence?, Remote Sensing of Environment, 166, 8–21, doi:10.1016/j.rse.2015.06.002, 2015.

Verrelst, J., van der Tol, C., Magnani, F., Sabater, N., Rivera, J. P., Mohammed, G. and Moreno, J.: Evaluating the predictive power of sun-induced chlorophyll fluorescence to estimate net photosynthesis of vegetation canopies: A SCOPE modeling study, Remote Sensing of Environment, 176, 139–151, doi:10.1016/j.rse.2016.01.018, 2016.

Walther, S., Voigt, M., Thum, T., Gonsamo, A., Zhang, Y., Köhler, P., Jung, M., Varlagin, A. and Guanter, L.: Satellite chlorophyll fluorescence measurements reveal large-scale decoupling of photosynthesis and greenness dynamics in boreal evergreen forests, Global Change Biology, 22(9), 2979–2996, doi:10.1111/gcb.13200, 2016.

Wang, S., Huang, C., Zhang, L., Lin, Y., Cen, Y. and Wu, T.: Monitoring and Assessing the 2012 Drought in the Great Plains: Analyzing Satellite-Retrieved Solar-Induced Chlorophyll Fluorescence, Drought Indices, and Gross Primary Production, Remote Sensing, 8(2), 61, doi:10.3390/rs8020061, 2016.

Wu, C., Niu, Z., Tang, Q. and Huang, W.: Estimating chlorophyll content from hyperspectral vegetation indices: Modeling and validation, Agricultural and Forest Meteorology, 148(8), 1230–1241, doi:10.1016/j.agrformet.2008.03.005, 2008.

Yang, P. and van der Tol, C.: Linking canopy scattering of far-red sun-induced chlorophyll fluorescence with reflectance, Remote Sensing of Environment, 209, 456–467, doi:10.1016/j.rse.2018.02.029, 2018.

Zhang, Q., Xiao, X., Braswell, B., Linder, E., Baret, F. and Mooreiii, B.: Estimating light absorption by chlorophyll, leaf and canopy in a deciduous broadleaf forest using MODIS data and a radiative transfer model, Remote Sensing of Environment, 99(3), 357–371, doi:10.1016/j.rse.2005.09.009, 2005.

Zhang, Q., Middleton, E. M., Cheng, Y.-B., Huemmrich, K. F., Cook, B. D., Corp, L. A., Kustas, W. P., Russ, A. L., Prueger, J. H. and Yao, T.: Integrating chlorophyll fAPAR and nadir photochemical reflectance index from EO-1/Hyperion to predict cornfield daily gross primary production, Remote Sensing of Environment, 186, 311–321, doi:10.1016/j.rse.2016.08.026, 2016a.

Zhang, Y., Peng, C., Li, W., Fang, X., Zhang, T., Zhu, Q., Chen, H. and Zhao, P.: Monitoring and estimating drought-induced impacts on forest structure, growth, function, and ecosystem services using remote-sensing data: recent progress and future challenges, Environmental Reviews, 21(2), 103–115, 2013.

Zhang, Y., Guanter, L., Berry, J. A., Joiner, J., van der Tol, C., Huete, A., Gitelson, A., Voigt, M. and Köhler, P.: Estimation of vegetation photosynthetic capacity from space-based measurements of chlorophyll fluorescence for terrestrial biosphere models, Global Change Biology, 20(12), 3727–3742, doi:10.1111/gcb.12664, 2014.

Zhang, Y., Xiao, X., Jin, C., Dong, J., Zhou, S., Wagle, P., Joiner, J., Guanter, L., Zhang, Y., Zhang, G., Qin, Y., Wang, J. and Moore, B.: Consistency between sun-induced chlorophyll fluorescence and gross primary production of vegetation in North America, Remote Sensing of Environment, 183, 154–169, doi:10.1016/j.rse.2016.05.015, 2016b.

Zhang, Y., Guanter, L., Berry, J. A., van der Tol, C., Yang, X., Tang, J. and Zhang, F.: Model-based analysis of the relationship between sun-induced chlorophyll fluorescence and gross primary production for remote sensing applications, Remote Sensing of Environment, 187, 145–155, doi:10.1016/j.rse.2016.10.016, 2016c.

Zhang, Y., Xiao, X., Wu, X., Zhou, S., Zhang, G., Qin, Y. and Dong, J.: A global moderate resolution dataset of gross primary production of vegetation for 2000–2016, Scientific Data, 4, 170165, doi:10.1038/sdata.2017.165, 2017a.

Zhang, Y., Song, C., Band, L. E., Sun, G. and Li, J.: Reanalysis of global terrestrial vegetation trends from MODIS products: Browning or greening?, Remote Sensing of Environment, 191, 145–155, doi:10.1016/j.rse.2016.12.018, 2017b.

Zhang, Y., Xiao, X., Zhang, Y., Wolf, S., Zhou, S., Joiner, J., Guanter, L., Verma, M., Sun, Y., Yang, X., Paul-Limoges, E., Gough, C. M., Wohlfahrt, G., Gioli, B., van der Tol, C., Yann, N., Lund, M. and de Grandcourt, A.: On the relationship between sub-daily instantaneous and daily total gross primary production: Implications for interpreting satellite-based SIF retrievals, Remote Sensing of Environment, 205, 276–289, doi:10.1016/j.rse.2017.12.009, 2018a.

Zhang, Y., Joiner, J., Gentine, P. and Zhou, S.: Reduced solar-induced chlorophyll fluorescence from GOME-2 during Amazon drought caused by dataset artifacts, Global Change Biology, doi:10.1111/gcb.14134, 2018b.

Zhang, Y., Xiao, X., Wolf, S., Wu, J., Wu, X., Gioli, B., Cescatti, A., Van Der Tol, C., Zhou, S., Gough, C., Gentine, P., Zhang, Y., Steinbrecher, R. and Ardö, J.: Spatio-temporal convergence of maximum daily light-use efficiency based on radiation absorption by canopy chlorophyll, Geophysical Research Letters, (45), 3508–3519, doi:10.1029/2017GL076354, 2018c.

Zhao, M., Heinsch, F. A., Nemani, R. R. and Running, S. W.: Improvements of the MODIS terrestrial gross and net primary production global data set, Remote Sensing of Environment, 95(2), 164–176, doi:10.1016/j.rse.2004.12.011, 2005.

Zhu, X. X., Tuia, D., Mou, L., Xia, G. S., Zhang, L., Xu, F. and Fraundorfer, F.: Deep Learning in Remote Sensing: A Comprehensive Review and List of Resources, IEEE Geoscience and Remote Sensing Magazine, 5(4), 8–36, doi:10.1109/MGRS.2017.2762307, 2017.

Zhu, Z., Piao, S., Myneni, R. B., Huang, M., Zeng, Z., Canadell, J. G., Ciais, P., Sitch, S., Friedlingstein, P., Arneth, A., Cao, C., Cheng, L., Kato, E., Koven, C., Li, Y., Lian, X., Liu, Y., Liu, R., Mao, J., Pan, Y., Peng, S., Peñuelas, J., Poulter, B., Pugh, T. A. M., Stocker, B. D., Viovy, N., Wang, X., Wang, Y., Xiao, Z., Yang, H., Zaehle, S. and Zeng, N.: Greening of the Earth and its drivers, Nature Climate Change, 6(8), 791–795, doi:10.1038/nclimate3004, 2016.

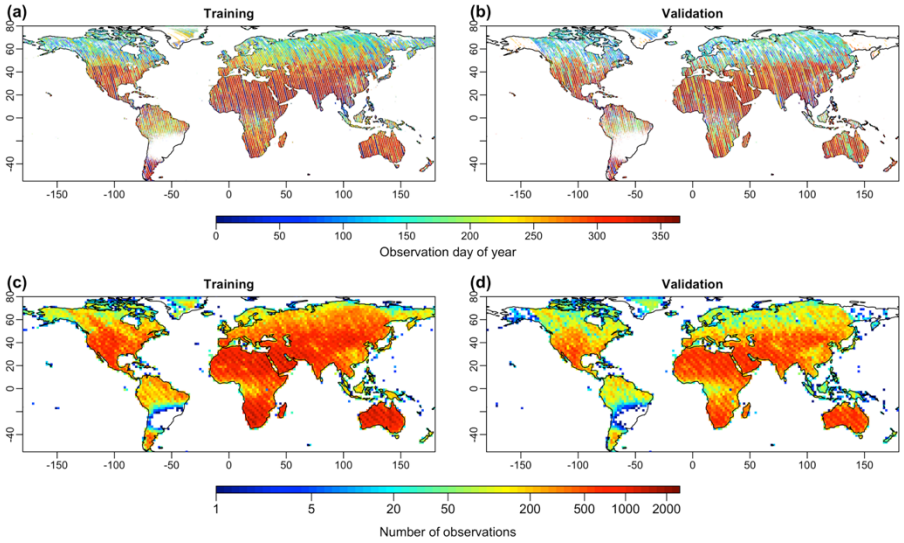


**Figure 1. Samples that were used for NN training (year 2015 and 2016) and validation (2014 and 2017). Upper panel shows the spatial distribution of observation day of year (DOY) and the bottom panel shows the spatial distribution of the sample density. Each point in (a,c) represents a 0.05-degree training gridcell. Limited observations in South America were caused by the South Atlantic Anomaly (Sun et al., 2018).**

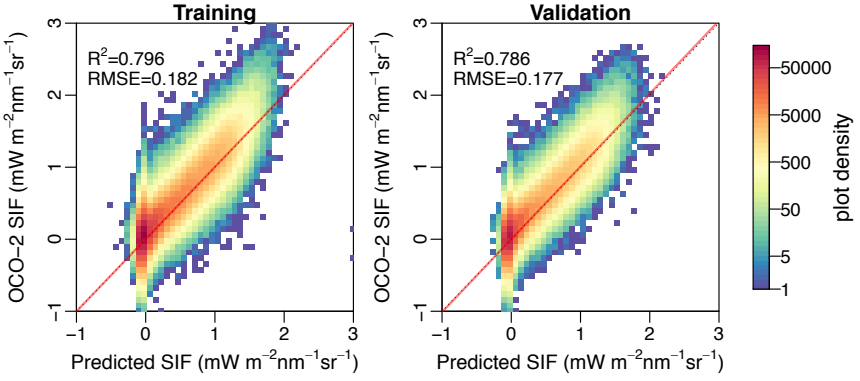

**Figure 2. Predicted SIF in comparison with the OCO-2 SIF. Red lines represent the regression slope and the black dotted lines represent the 1:1 line.**

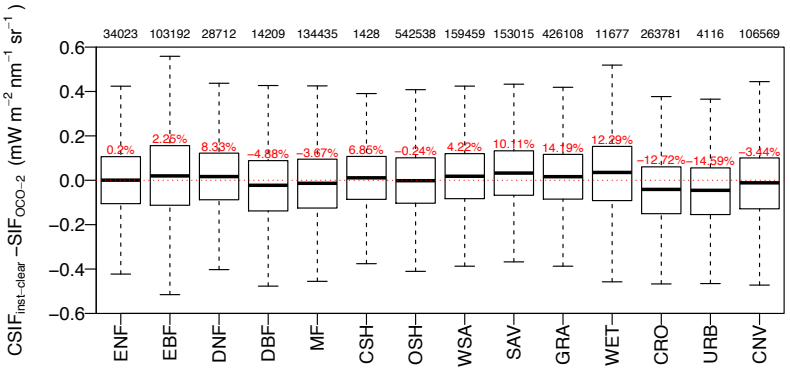


**Figure 3. Difference between $CSIF_{clear-inst}$ with $SIF_{OCO-2}$ for major biome types during 2014-2017. The MODIS land cover dataset for 2010 was used to identify the land cover type for each 0.05° grid (Friedl et al., 2010). The red percentages above each box represent the mean relative error, and the numbers on top of the figure frame represent the total sample numbers for each biome type. Abbreviations: ENF, evergreen needleleaf forest; EBF, evergreen broadleaf forest; DNF, deciduous needleleaf forest; DBF, deciduous broadleaf forest; MF, mixed forest; CSH, closed shrubland; OSH, open shrubland; WSA, woody savannas; SAV, savannas; GRA, grassland; WET, wetland; CRO, cropland; URB, urban; CNV, cropland or natural vegetation mosaics.**

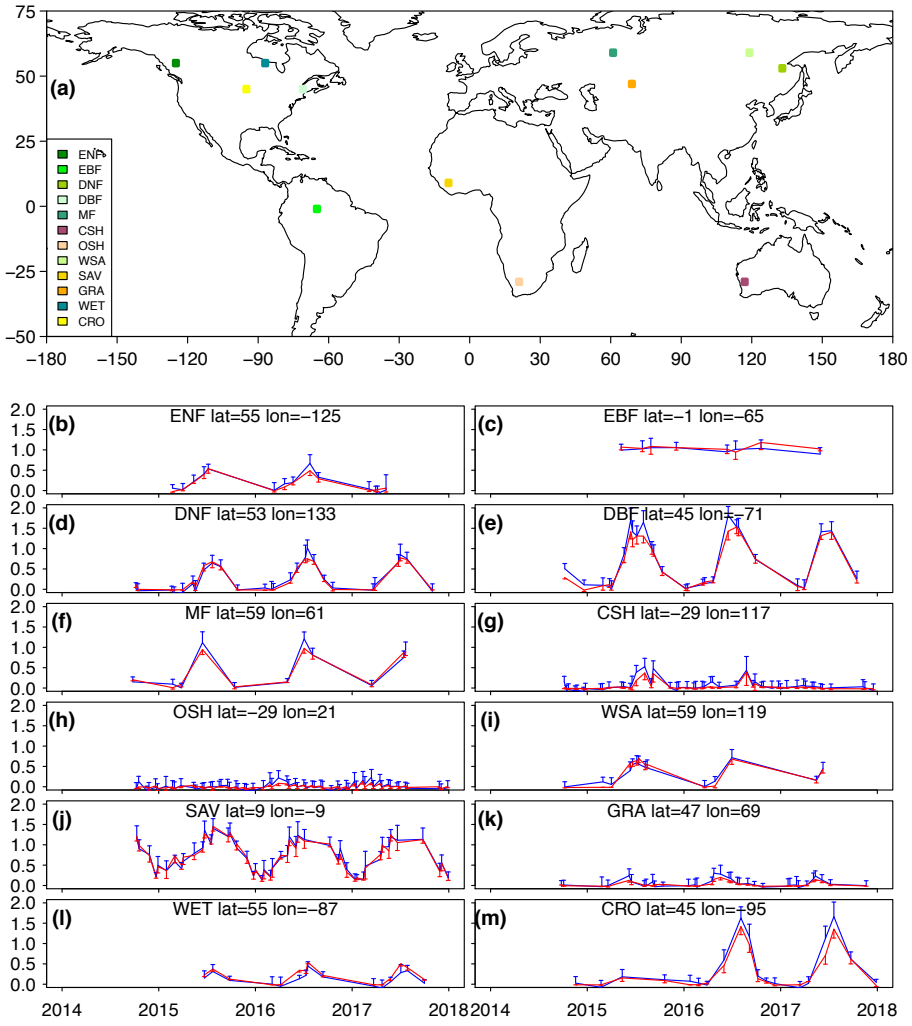


**Figure 4. Comparison of predicted SIF by NN and OCO-2 observed SIF for 12 samples (2° ×2°) of major vegetated land cover types during 2014 to 2017. All samples in the training and validation are used. The blue color represents the observed SIF by OCO-2 and the red color represent the SIF prediction by NN. The error bars represent the standard deviation of all 0.05° ×0.05° samples used to generate the 2° ×2° gridboxes. MODIS MOD12C1 V6 land cover dataset is used to select these sample gridboxes.**

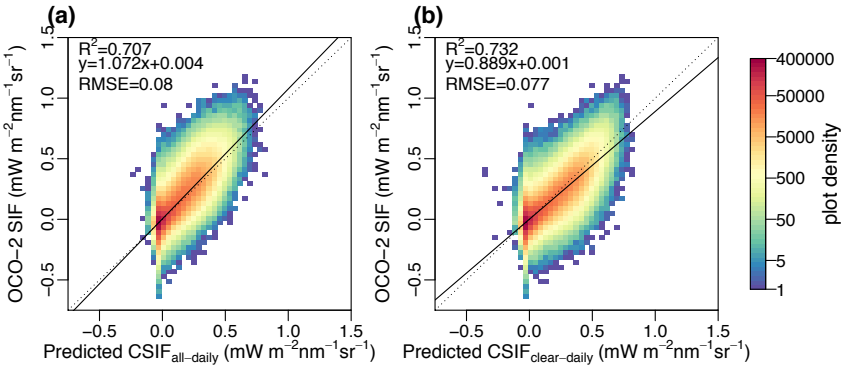


**Figure 45. Comparison between the retrieved SIF and the (a) predicted all-sky daily CSIF and (b) clear-sky daily CSIF. The instantaneous SIF retrievals from OCO-2 were converted to daily average values for comparison.**

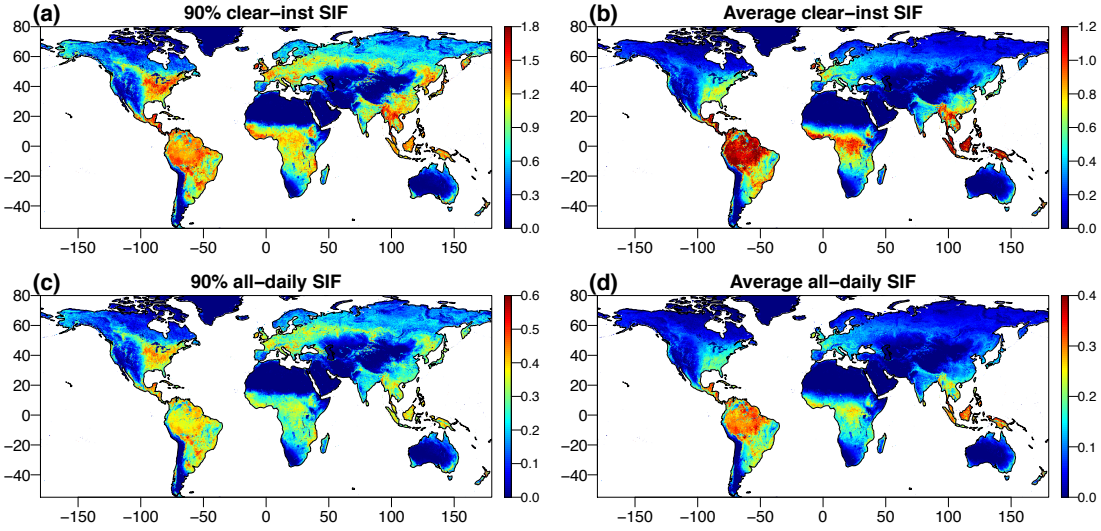


**Figure 56. Spatial pattern of maximum (90 percentile) and average daily values for instantaneous clear-sky SIF and all-sky daily SIF. All values are in the unit of mW $m^{-2}$ $nm^{-1}$ $sr^{-1}$.**

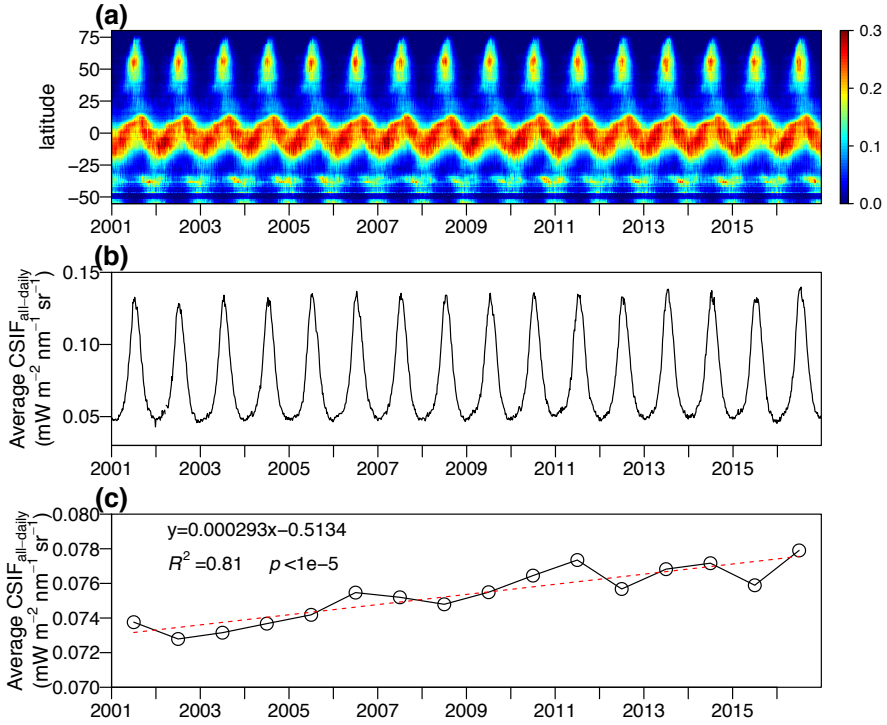


**Figure 6~~7~~. Seasonal and inter-annual variation of all-sky condition daily CSIF ($CSIF_{all\text{-}daily}$). (a) the latitudinal averages of $CSIF_{all\text{-}daily}$ for each 4-day (in mW $m^{-2}$ $nm^{-1}$ $sr^{-1}$). (b) global average of $CSIF_{all\text{-}daily}$ for each 4-day. (c) the annual average $CSIF_{all\text{-}daily}$ between 2001 to 2016 (black line) with linear fit (red dashed line).**

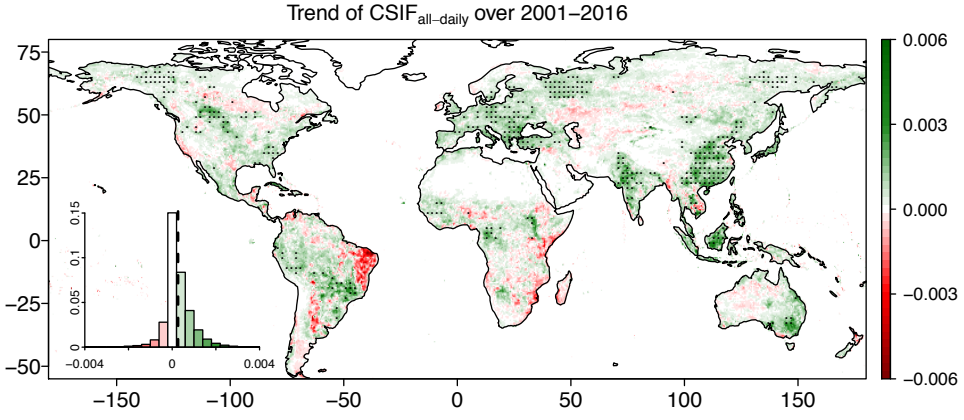

**Figure ~~7~~8. Trend of annual average $CSIF_{all\text{-}daily}$ during 2003-2016. The trend is calculated by the Sen's Slope estimator. Dots represent the trend is significant ($p<0.05$) through a Mann-Kendall test. Inset in bottom left shows the histogram of the $CSIF_{all\text{-}daily}$ trend. Dashed vertical line represents the average trend. Barren areas with an annual average $CSIF_{all\text{-}daily}$ smaller than 0.006 mW $m^{-2}$ $nm^{-1}$ $sr^{-1}$ are screened from analysis. Trends are in the units of mW $m^{-2}$ $nm^{-1}$ $sr^{-1}$ $yr^{-1}$.**

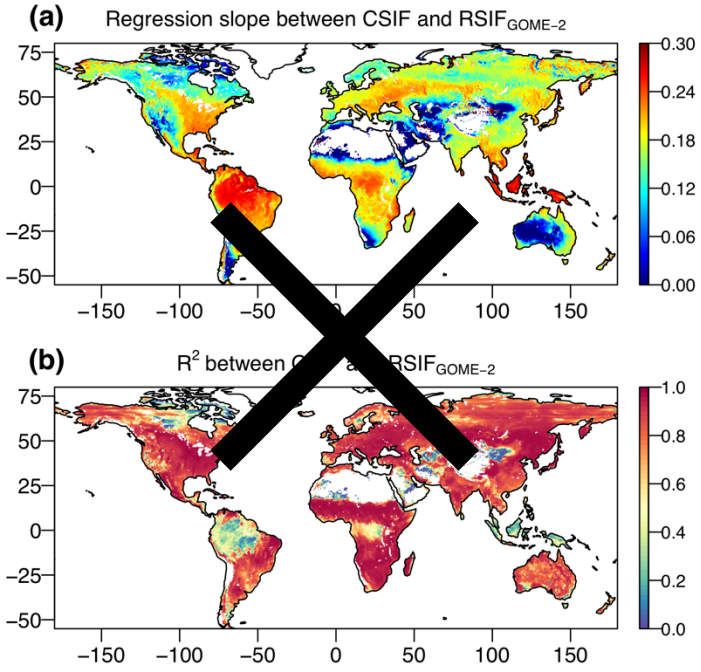
(a)
Regression slope between CSIF and RSIF$_{GOME-2}$
75
50
25
0
−25
−50
−150
−100
−50
50
100
150
0.30
0.24
0.18
0.12
0.06
0.00
(b)
$R^2$ between C
RSIF$_{GOME-2}$
1.0
0.8
0.6
0.4
0.2
0.0

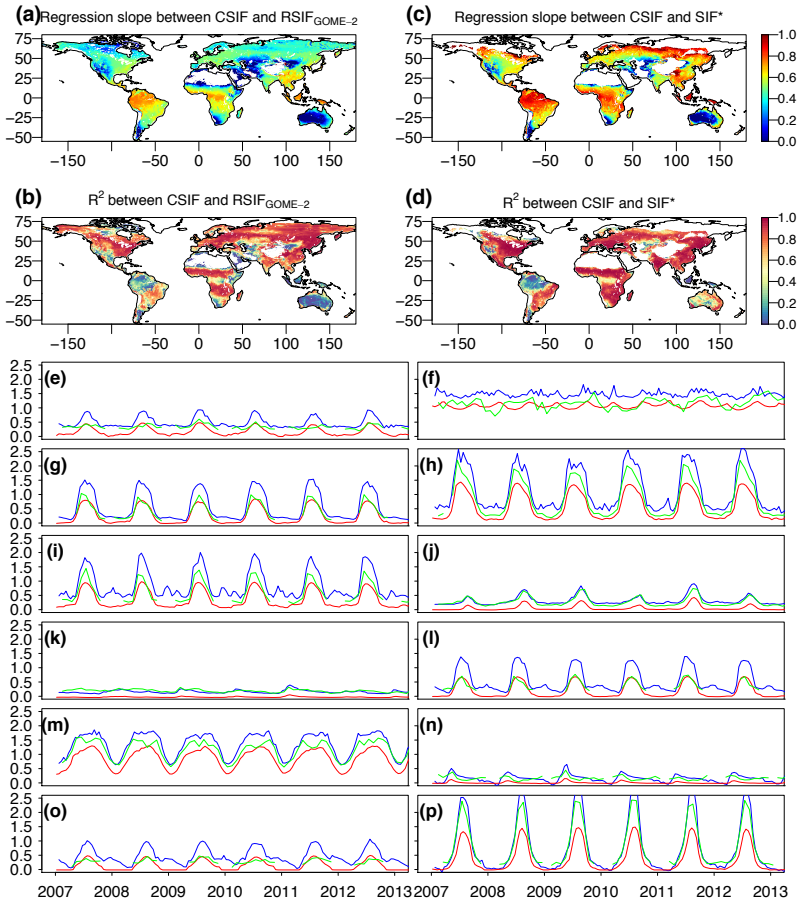


**Figure ~~8~~9. Comparison between CSIF, RSIF$_{GOME-2}$ and SIF* dataset. Regression slopes and coefficient of determination ($R^2$) between the ~~continuous~~contiguous ~~all~~clear-sky condition ~~daily~~ instantaneous SIF from OCO-2 (CSIF$_{inst\text{-}clear}$~~$_{all\text{-}daily}$~~) and the reconstructed SIF from GOME-2 (RSIF$_{GOME-2}$ a, b) or SIF* (c, d) dataset. The regressions are forced to pass the origin. The CSIF$_{clear\text{-}inst}$~~$_{all\text{-}daily}$~~ is aggregated to semi-monthly and $0.5° \times 0.5°$ spatial resolution to be consistent with RSIF$_{GOME-2}$. Comparison uses the data between 2007 to 2016 (RSIF) or 2007 to 2013 (SIF*). White regions are barren regions ~~identified by the RSIF$_{GOME-2}$ dataset~~. (e-p) Time series comparison among CSIF (red), RSIF$_{GOME-2}$ (blue) and SIF* (green) for pixels in 12 major land cover types shown in Figure 4.**

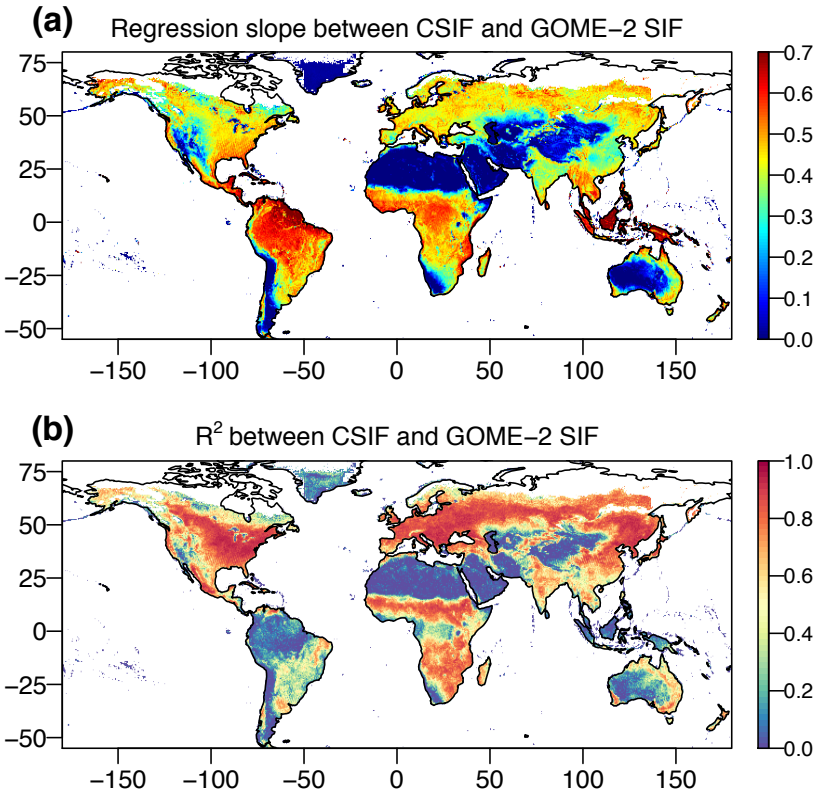


**Figure ~~9~~10. Regression slopes and coefficient of determination ($R^2$) between the ~~continuous~~contiguous all-sky condition daily SIF from OCO-2 ($CSIF_{all\text{-}daily}$) and the satellite-retrieved daily SIF from GOME-2 ($SIF_{GOME\text{-}2}$). The regressions are forced to pass through the origin. The $CSIF_{all\text{-}daily}$ is aggregated to monthly and $0.5° \times 0.5°$ spatial resolution to be consistent with $SIF_{GOME\text{-}2}$. Comparison uses the data between 2007 to 2016.**

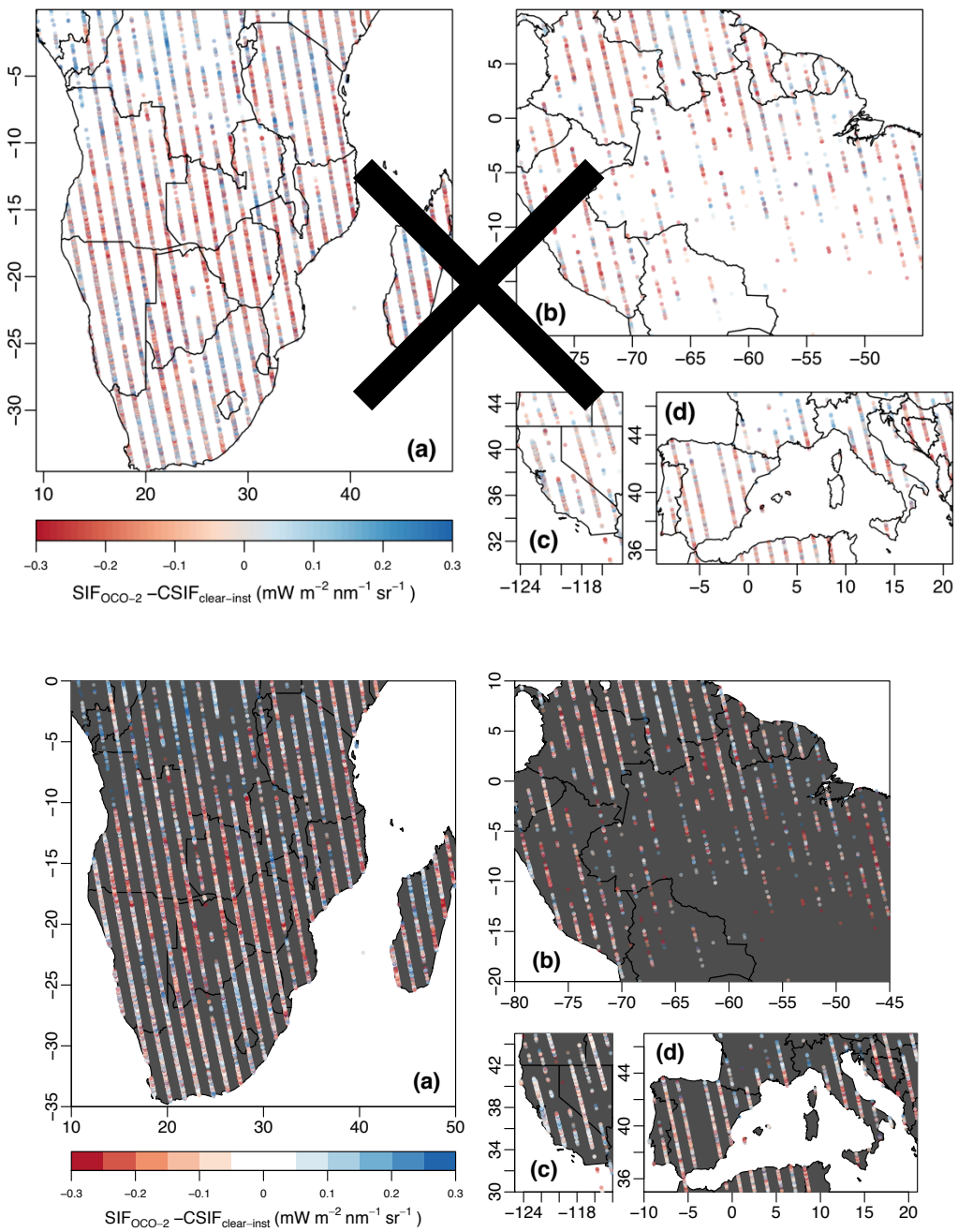


**Figure ~~10~~11. Difference between the OCO-2 SIF and CSIF$_{clear-inst}$ for 4 specific drought events during 2014-2017. (a) Southern Africa drought between October, 2015 and February, 2016. (b) Northeast Amazon drought between January and March, 2016. (c) California drought between January and March, 2015. (d) Southern Europe drought between July and August, 2017.**

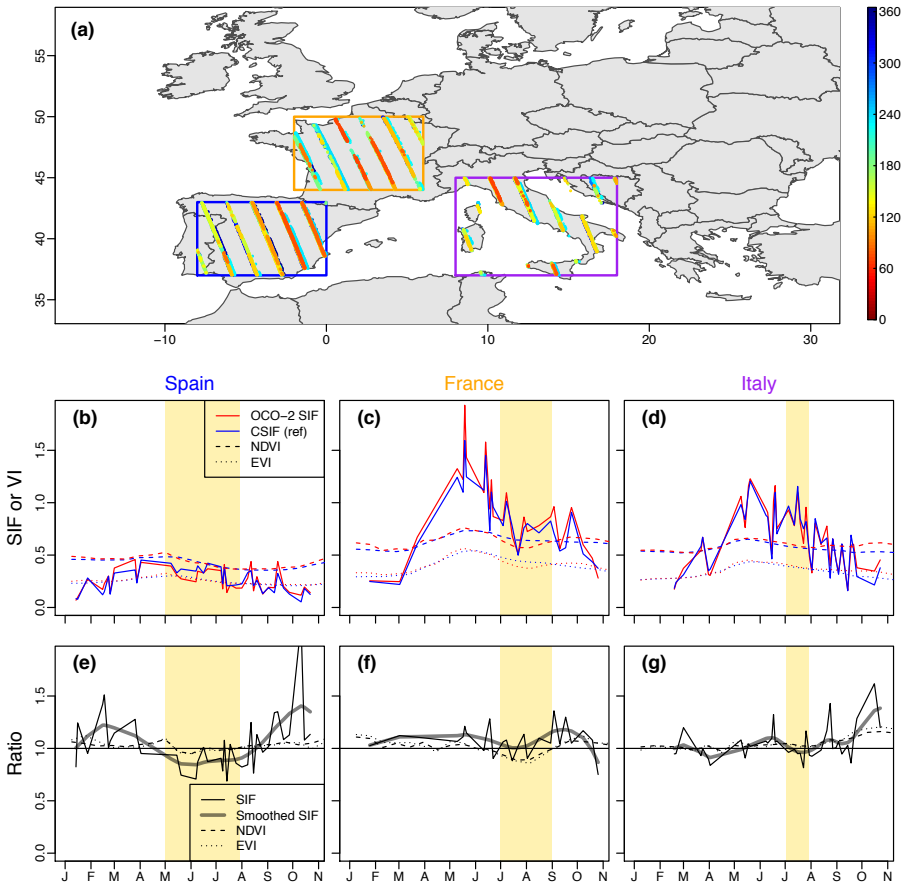


**Figure 12~~1~~. (a) Spatial distribution of OCO-2 SIF observations during January 1st to November 1st in 2015. Different colours represent the observation day of year (DOY). (b-d) average OCO-2 SIF, CSIF NDVI and EVI for the three countries as indicated by three boxes in (a). For two vegetation indices, red colour represents the observations in 2015 and blue colour represents multi-year average (2000-2014). (e-g) the ratio between OCO-2 SIF and CSIF (SIF) or vegetation indices in 2015 and multi-year average. Thick grey line presents the splines smoothed SIF ratio.**

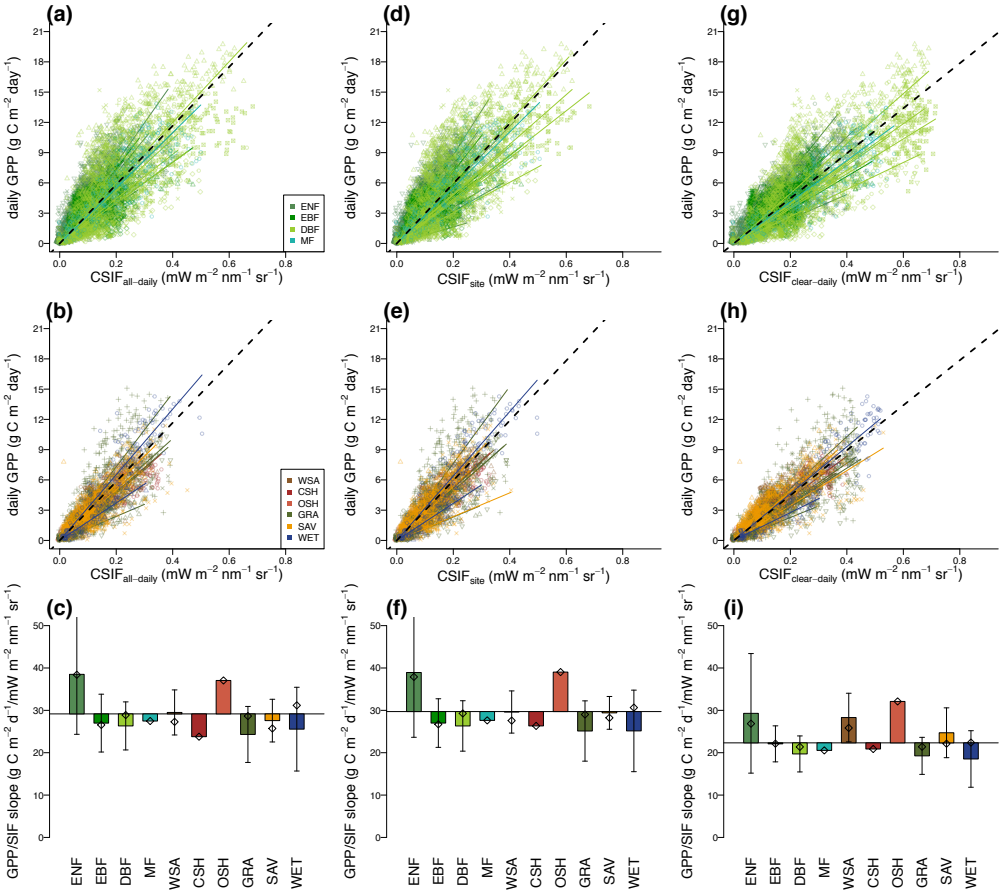


**Figure ~~12~~13. Comparison between GPP estimates from 40 EC flux towers and CSIF$_{all-daily}$ (a-c) that uses BESS PAR, CSIF$_{site}$ (d-f) that uses site-measured radiation and CSIF$_{clear-daily}$ (g-i) that assume clear-sky condition. The 40 sites were grouped into forest (a,d,g) and non-forests (b,e,h). Colours-symbols combinations represent different sites. Summary of the regression slopes between GPP and CSIF for different land cover types (c,f,i). The baseline (dashed black lines) was calculated using all samples (29.71 for CSIF$_{all-daily}$ 29.18 for CSIF$_{site}$ and 22.33 for CSIF$_{clear-daily}$). Error bars represent the standard deviation of slopes across sites within this biome type. Rhombuses represent regression for each biome type when data from all sites were combined.**

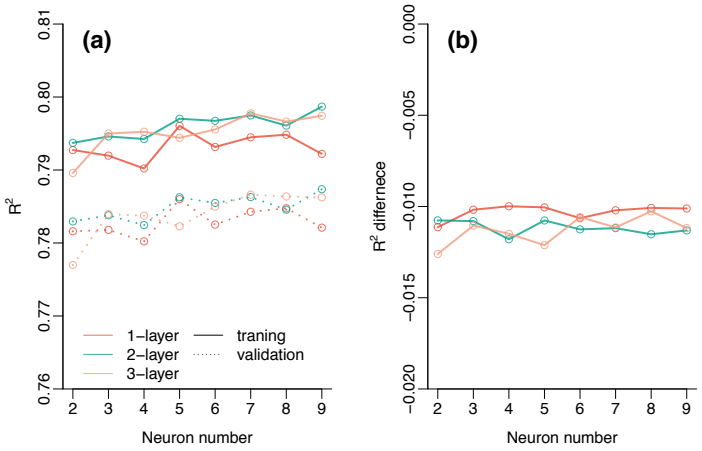


**Figure A1. (a) Comparison of model performance ($R^2$) during training and validation with a variety of NN layers (1-3) and neuron numbers for each layer (1-8). (b) difference of model performance between the training and validation for different layer and neuron combinations.**